Elastic scattering theory and transport in graphene

D. S. Novikov
W. I. Fine Institute of Theoretical Physics, University of Minnesota, Minneapolis, Minnesota 55455, USA
and Department of Electrical Engineering and Department of Physics, Princeton University, Princeton, New Jersey 08544, USA
(Received 8 July 2007; revised manuscript received 4 October 2007; published 28 December 2007)

Electron properties of graphene are described in terms of Dirac fermions. Here we thoroughly outline the elastic scattering theory for the two-dimensional massive Dirac fermions in the presence of an axially symmetric potential. While the massless limit is relevant for pristine graphene, keeping finite mass allows for generalizations onto situations with broken symmetry between the two sublattices and provides a link to the scattering theory of electrons in a parabolic band. We demonstrate that the Dirac theory requires short-distance regularization for potentials which are more singular than $1/r$. The formalism is then applied to scattering off a smooth short-ranged potential. Next, we consider the Coulomb potential scattering, where the Dirac theory is consistent for a point scatterer only for the effective impurity strength below $1/2$. From the scattering phase shifts we obtain the exact Coulomb transport cross section in terms of the impurity strength. The results are relevant for transport in graphene in the presence of impurities that do not induce scattering between the Dirac points in the Brillouin zone.

DOI: 10.1103/PhysRevB.76.245435 PACS number(s): 81.05.Uw, 72.10.−d, 73.63.−b, 73.40.−c

INTRODUCTION AND OUTLINE

Graphene, a layer of carbon atoms arranged in a honeycomb lattice, has been long known for its peculiar electronic dispersion, equivalent to that of massless two-dimensional (2D) Dirac fermions. This system was first considered in tight-binding approximation by Wallace[1] and by McClure.[2] For a long time, graphene monolayer served as a low-dimensional toy model where Dirac fermions appear naturally.[4,5] Significant interest to this material arose in 1990s fueled by the discovery of carbon nanotubes.[3] The field has experienced an even stronger surge of interest since 2004, when graphene monolayers were obtained experimentally.[6] The outstanding quality of graphene monolayers and few-layered samples is manifest in high mobility resulting in ballistic conductance on micrometer scale and in quantized Hall effect.[6–10]

Recent electron transport measurements[7–9] show that the mobility in graphene is approximately independent of the carrier density (i.e., conductivity grows proportional to the density). The effects of various kinds of the potential disorder on transport in graphene have been considered in a number of works.[11–27] Arguably, the density-independent mobility originates mainly due to the Coulomb impurities in the substrate.[15–17]

The importance of the smooth potential disorder for the transport in graphene prompts the development of the scattering theory for the 2D Dirac fermions, both massless and massive. Physically, a nonzero mass can arise due to an external perturbation that distinguishes between the sublattices; recent *ab initio* density functional calculations predict the Dirac gap of 53 meV when placing graphene monolayer on a hexagonal boron nitride substrate.[28] Somewhat similar perturbation occurs in bilayer graphene,[29–31] although in this example, the spectrum is not exactly of the Dirac form. An interesting possibility for the Dirac gap opening up due to the spin-orbit coupling was considered by Kane and Mele.[32]

The purpose of this work is to thoroughly outline the elastic scattering theory for 2D Dirac fermions in the axially symmetric potentials. Such a 2D formalism is built essentially following Ref. 33, the classic reference for scattering in three-dimensional (3D) Dirac systems. The connection to the transport in graphene in the presence of potential centers whose field is smooth on the lattice scale is established via the transport cross section.

We start from the basic facts about the 2D Dirac model and write the normalized spinor plane and spherical waves (Sec. I). In Sec. II, we study the properties of the radial solutions for the 2D Dirac spinors, define the scattering phase shifts, and link them to the differential and transport cross sections. We also derive the Born approximation for the 2D Dirac spinors, as well as outline analytical properties of the radial solutions on the complex energy plane.

One of the observations made in Sec. II is that the Dirac problem, both massive and massless, requires a short-distance regularization whenever the external potential is more singular than $1/r$. Classically, this corresponds to falling into the potential center. For such singular potentials, the purely Dirac formalism is inapplicable, and the lattice-scale physics starts playing a role.

In Sec. III, we consider scattering off a potential localized within a finite radius that exceeds the lattice constant but is smaller than the particle wavelength.

In Sec. IV, we focus on one of the most important scattering problems for graphene — that for the potential $U=-\hbar v\alpha/r$. The latter problem has so far been treated in the Born approximation.[15–17] The exact solution is presented in detail for both massless and massive cases and for both signs of the impurity charge α. The asymptotic behavior of the scattering solutions and scattering phase shifts are studied, with the particular attention paid to the "ultra-relativistic" and "nonrelativistic" limits, relevant correspondingly for the pristine graphene and for the graphene layer with broken sublattice symmetry, or for the electrons in a semiconductor with a parabolic band.

The $1/r$ problem deserves a special consideration, as it is a borderline case for the falling into the potential center. It has been known[34] that the solutions in the $1/r$ potential be-

come singular whenever the "fine structure constant" $\alpha > \alpha_c = 1/2$, i.e., at even smaller value than that in 3D ($\alpha_c = 1$). In this respect, the physics of the Coulomb impurity in graphene, depending on the dielectric environment, may correspond to the "supercritical" relativistic heavy atom (that with $Z > 137$).[35–38]

Finally, in Sec. V, we use the exact scattering phases to calculate the transport cross section for the subcritical Coulomb impurity and compare the exact result with the Born approximation. Our main finding there is that, for a given carrier charge, the attracting impurity scatters more effectively than the repelling one. This should be contrasted with known exact 2D and 3D nonrelativistic scattering results in a $1/r$ potential, where such an asymmetry does not take place.

I. FREE ELECTRONS IN GRAPHENE

A. Model

The key features of electron dispersion in an ideal graphene monolayer can be summarized as follows.[3] With the two sites per unit cell, graphene's π electron band has the two inequivalent points in the Brillouin zone, at which the electron and hole subbands just barely touch. At these so-called Dirac points K and K', the carrier dispersion is linear and electron-hole symmetric, $\epsilon(\mathbf{p}) \propto \pm p$. Separately at the K and K' points, the wave function in the effective-mass approximation has a spinor structure, its two components corresponding to the two sublattices. This spinor obeys the massless Dirac equation. The low-energy states near the K and K' points are decoupled in a pristine graphene monolayer. Provided the material is subject to external fields that are adiabatic on the lattice scale, the low-energy properties can be understood in terms of the $N_f = 2_{\text{spin}} \times 2_{\text{valley}} = 4$ independent Dirac fermion polarizations.

Near a given Dirac point, the free effective-mass Hamiltonian is

$$\mathcal{H}_0 = -i\hbar v(\tau_3 \sigma_1 \partial_x + \sigma_2 \partial_y) + \Delta \sigma_3, \tag{1.1}$$

where $v \approx 1 \times 10^6$ m/s is the graphene Fermi velocity, $\sigma_{1,2,3}$ are the Pauli matrices that act in the spinor space corresponding to the two sublattices of a honeycomb lattice, while $\tau_3 = \pm 1$ distinguishes between the K and K' Dirac points. Everywhere in this work, we consider the dynamics on the scale much larger than the graphene's lattice constant and neglect scattering between the Dirac points. Hence, without loss of generality, we set $\tau_3 = +1$ in what follows.

In the Hamiltonian (1.1), we also introduced the gap (the Dirac mass)

$$\Delta \equiv Mv^2. \tag{1.2}$$

Although this term is absent by symmetry in an ideal graphene monolayer, it can become important when the symmetry is reduced. Without loss of generality here, we set $M > 0$ (working at zero magnetic field, we are not concerned with the parity anomaly effects.[4,5])

The Hamiltonian (1.1) corresponds to the Lagrangian ($\hbar = v = 1$, $\tau_3 = +1$)

$$\mathcal{L}_0 = \bar{\psi}(i\gamma^\mu \partial_\mu - M)\psi, \quad \bar{\psi} \equiv \psi^\dagger \gamma^0, \tag{1.3}$$

where the Dirac matrices $\gamma^0 = \sigma_3$, $\gamma^1 = i\sigma_2$, and $\gamma^2 = -i\sigma_1$, such that $\{\gamma^\mu, \gamma^\nu\} = 2g^{\mu\nu}$, with $g^{\mu\nu} = \text{diag}(1, -1, -1)$. In this "relativistic" notation, the Lorentz-invariant fermion current is

$$J^\mu = \bar{\psi}\gamma^\mu \psi = (\rho, \mathbf{J}), \tag{1.4}$$

where the number density and the current are

$$\rho = \psi^\dagger \psi, \quad \mathbf{J} = \psi^\dagger \boldsymbol{\sigma} \psi, \tag{1.5}$$

with $\boldsymbol{\sigma} = (\sigma_1, \sigma_2)$.

B. Spinor plane waves

Consider the eigenproblem $\mathcal{H}_0 \psi = \epsilon \psi$, Eq. (1.1), where we represent the two-component spinor

$$\psi(\mathbf{r}) = \begin{pmatrix} \varphi \\ \chi \end{pmatrix}. \tag{1.6}$$

The components of ψ satisfy (we set $\hbar = v = 1$ in what follows)

$$\begin{pmatrix} M & p_x - ip_y \\ p_x + ip_y & -M \end{pmatrix} \begin{pmatrix} \varphi \\ \chi \end{pmatrix} = \epsilon \begin{pmatrix} \varphi \\ \chi \end{pmatrix}, \tag{1.7}$$

where $p_x = -i\partial_x$ and $p_y = -i\partial_y$. In the plane wave basis $(\varphi\ \chi)^T = u_{\epsilon,\mathbf{p}} e^{i\mathbf{pr}}$, the differential operators become components of the momentum eigenvalue $\mathbf{p}$, yielding the relativistic dispersion

$$\epsilon = \pm\sqrt{p^2 + M^2}, \quad p = \sqrt{p_x^2 + p_y^2}, \tag{1.8}$$

where $\pm$ distinguishes between the particle and hole sectors. The conventional normalization "one particle in a unit volume"[33] $J^\mu = p^\mu/\epsilon = (1, \mathbf{v}_\mathbf{p})$, where $\mathbf{v}_\mathbf{p} = \partial\epsilon/\partial\mathbf{p} = \mathbf{p}/\epsilon$ is the velocity, requires $\bar{\psi}_{\epsilon,\mathbf{p}} \psi_{\epsilon,\mathbf{p}} \equiv M/\epsilon$ or, equivalently, $\psi^\dagger_{\epsilon,\mathbf{p}} \psi_{\epsilon,\mathbf{p}} = 1$, yielding

$$\psi_{\epsilon;\mathbf{p}} = u_{\epsilon;\mathbf{p}} e^{i\mathbf{pr}}, \quad u_{\pm|\epsilon|;\mathbf{p}} = \frac{w}{\sqrt{2|\epsilon|}} \begin{pmatrix} \sqrt{|\epsilon + M|} \\ \pm\sqrt{|\epsilon - M|} e^{i\theta_\mathbf{p}} \end{pmatrix}. \tag{1.9}$$

Here $\theta_\mathbf{p} = \arg(p_x + ip_y)$ and the upper and lower signs refer to the electron ($\epsilon > M$) and hole ($\epsilon < -M$) parts of the spectrum, $\pm \equiv \text{sgn}\,\epsilon$. The absolute values under the square roots are introduced to describe both sectors. The factor $w = e^{i\phi}$ is an overall phase that has a meaning of the nonrelativistic particle's wave function in the rest frame, $\epsilon = M$.

C. Spinor spherical waves

For the purpose of developing the scattering theory, below we introduce the spherical wave basis of eigenstates of the problem (1.1).

First recall that the 2D nonrelativistic scalar particle with fixed absolute value of the momentum $p = |\mathbf{p}|$ and fixed projection $m = 0, \pm 1, \pm 2, \ldots$, of angular momentum on the z axis (perpendicular to the plane) is described by the spherical wave

$$\Psi_{pm}(\mathbf{r}) = \Phi_m(\theta) R_{pm}(r). \tag{1.10}$$

Here, the angular harmonics

$$\Phi_m = \frac{1}{\sqrt{2\pi}} e^{im\theta}, \quad m = 0, \pm 1, \pm 2, \ldots, \tag{1.11}$$

and the radial functions $R_{pm}(r)$ satisfy the radial Schrödinger equation

$$-\frac{1}{r}\frac{d}{dr}\left(r\frac{d}{dr}R_{pm}\right) + \frac{m^2}{r^2}R_{pm} = p^2 R_{pm}, \tag{1.12}$$

which reduces to the Bessel equation

$$\rho^2 R''_{\rho\rho} + \rho R'_\rho + (\rho^2 - m^2)R = 0, \quad \rho = pr. \tag{1.13}$$

The solutions are the Bessel functions $J_m(\rho)$ and the Neumann functions $Y_m(\rho)$, whose asymptotic behavior

$$J_m(\rho \gg m) \simeq \sqrt{\frac{2}{\pi\rho}} \cos\left(\rho - \frac{m\pi}{2} - \frac{\pi}{4}\right), \tag{1.14a}$$

$$Y_m(\rho \gg m) \simeq \sqrt{\frac{2}{\pi\rho}} \sin\left(\rho - \frac{m\pi}{2} - \frac{\pi}{4}\right). \tag{1.14b}$$

Their corresponding short-distance behavior is

$$J_m(pr) \sim \frac{1}{m!}\left(\frac{pr}{2}\right)^m \tag{1.15a}$$

$$\text{and } Y_m(pr) \sim \begin{cases} -\dfrac{\Gamma(m)}{\pi}\left(\dfrac{2}{pr}\right)^m, & m > 0 \\ \dfrac{2}{\pi}\ln(\gamma_E pr/2), & m = 0, \end{cases} \tag{1.15b}$$

where $\ln \gamma_E \simeq 0.577\cdots$ is the Euler's constant. [For $m<0$, use $J_{-m}=(-)^m J_m$ and $Y_{-m}=(-)^m Y_m$.] Thus, for the wave regular at $r=0$, one chooses $R_m \propto J_m(pr)$, normalized according to $\int_0^\infty r dr R_{pm} R_{p'm'} = 2\pi\delta_{mm'}\delta(p-p')$:

$$R_{pm} = \sqrt{2\pi p} J_m(pr) \sim \frac{2}{\sqrt{r}} \cos\left(pr - \frac{m\pi}{2} - \frac{\pi}{4}\right). \tag{1.16}$$

Coming back to the relativistic case, one notes that both the isospin $\frac{1}{2}\boldsymbol{\sigma}$ and the angular momentum $\hat{l}_z = -i\partial_\theta = -i(x\partial_y - y\partial_x)$ do not commute with the Hamiltonian (1.1):

$$[\hat{l}_z, \mathcal{H}_0] = i\boldsymbol{\sigma} \times \mathbf{p}, \quad \left[\tfrac{1}{2}\hat{\sigma}_z, \mathcal{H}_0\right] = -i\boldsymbol{\sigma} \times \mathbf{p}.$$

Thus, a state cannot be characterized by their values. (In fact, the spherical spinor components will have different eigenvalues of $\hat{l}_z$.) The conserved quantity is the "isospin-orbital" momentum around the $\hat{z}$ axis,[11]

$$\hat{j} = \hat{l}_z + \tfrac{1}{2}\sigma_z, \quad \hat{l}_z = -i\partial_\theta. \tag{1.17}$$

Also, similar to the 3D case,[33] the *parity* of a state is conserved: Under inversion $\mathbf{r} \to -\mathbf{r}$ (i.e., $\theta \to \theta + \pi$ for the polar angle and $\psi \to \gamma^0\psi$), the spinor components (1.6) transform as $\varphi(\mathbf{r}) \to \varphi(-\mathbf{r})$ and $\chi(\mathbf{r}) \to -\chi(-\mathbf{r})$. The spinor ψ_{pm} will have the definite parity $(-)^m$ if its components

$$\psi_{pm}(\mathbf{r}) = \begin{pmatrix} F_{pm}(r)\Phi_m(\theta) \\ iG_{pm}(r)\Phi_{m+1}(\theta) \end{pmatrix} \tag{1.18}$$

have the angular parts correspondingly with $l_z=m$ and $l_z=m+1$. The factor of i here is chosen for later convenience.

Consider now the radial parts $F_{pm}(r)$ and $G_{pm}(r)$ assuming $|\epsilon| > M$. From relations (1.7), it follows that

$$-\frac{1}{r}\frac{d}{dr}\left(r\frac{dF_{pm}}{dr}\right) + \frac{m^2}{r^2}F_{pm} = p^2 F_{pm}, \tag{1.19a}$$

$$-\frac{1}{r}\frac{d}{dr}\left(r\frac{dG_{pm}}{dr}\right) + \frac{(m+1)^2}{r^2}G_{pm} = p^2 G_{pm}. \tag{1.19b}$$

Equations (1.19a) and (1.19b) are of the radial Schrödinger form, Eq. (1.12). Thus, $F_{pm}=AR_{pm}(r)$ and $G_{pm}=BR_{p,m+1}(r)$. For the spinor wave regular at the origin, one chooses the radial functions in the form (1.16). To find A and B, we consider the limit $pr \to \infty$, when the wave function is approximately a plane wave in the direction of $\hat{\mathbf{r}}$. Using the asymptotic behavior (1.16) and relations (1.9) between the components of the plane wave, find $B/A = \pm\sqrt{|\epsilon - M|/|\epsilon + M|}$, where $\pm \equiv \operatorname{sgn}\epsilon$. Requiring the overall normalization $\int d^2\mathbf{r}\psi^\dagger_{pm}\psi_{p'm'} = 2\pi\delta_{mm'}\delta(p-p')$, we obtain the spinor spherical wave

$$\psi_{pm}(\mathbf{r}) = \frac{1}{\sqrt{2|\epsilon|}} \begin{pmatrix} \sqrt{|\epsilon + M|}R_{pm}(r)\Phi_m(\theta) \\ \pm i\sqrt{|\epsilon - M|}R_{p,m+1}(r)\Phi_{m+1}(\theta) \end{pmatrix}, \tag{1.20}$$

whose parity is $(-)^m$. Here, $R_{pm}(r) = \sqrt{2\pi p}J_m(pr)$ for the spinor regular at $r=0$, $R_{pm}(r) = \sqrt{2\pi p}Y_m(pr)$ for the spinor singular at $r=0$, and same applies for $R_{p,m+1}(r)$. The spinor (1.20) is also an eigenstate of operator (1.17) with the eigenvalue

$$j = m + \tfrac{1}{2}. \tag{1.21}$$

Below, we will often use eigenvalue (1.21) instead of the orbital number m to label states, eigenvalues, or phase shifts; e.g., for the spinors (1.20), $\psi_{pm}(\mathbf{r}) \equiv \psi_{pj}(\mathbf{r})$.

II. POTENTIAL SCATTERING

A. Equations for the radial functions

We consider elastic scattering off an axially symmetric external scalar potential $U(r)$. The Hamiltonian

$$\mathcal{H} = -i(\sigma_1\partial_x + \sigma_2\partial_y) + M\sigma_3 + U(r). \tag{2.1}$$

In the spinor components (1.6), Eq. (2.1) reads

$$\begin{aligned} (\epsilon - M - U)\varphi &= (p_x - ip_y)\chi, \\ (\epsilon + M - U)\chi &= (p_x + ip_y)\varphi, \end{aligned} \tag{2.2}$$

where $(p_x, p_y) = (-i\partial_x, -i\partial_y)$ are differential operators.

The crucial symmetry of problem (2.1) is the conservation of the total orbital momentum (1.17), since

$$[\hat{l}_z,\mathcal{H}]=-\left[\tfrac{1}{2}\hat{\sigma}_z,\mathcal{H}\right]=i\boldsymbol{\sigma}\times\mathbf{p}\Rightarrow[\hat{j}_z,\mathcal{H}]=0 \tag{2.3}$$

for any axially symmetric $U(r)$. This property allows us to work in the spherical basis of the form (1.18). Taking the spinor (1.6) in the form (1.18), and using $\Phi_{m+1}=e^{i\theta}\Phi_m$ and $p_x\pm ip_y=e^{\pm i\theta}\left(-i\partial_r\pm\frac{1}{r}\partial_\theta\right)$, where $\theta=\arg(x+iy)$, we obtain the following equations for the radial functions F and G:

$$\frac{dF}{dr}-\frac{m}{r}F+(\epsilon+M-U)G=0, \tag{2.4a}$$

$$\frac{dG}{dr}+\frac{m+1}{r}G-(\epsilon-M-U)F=0. \tag{2.4b}$$

Everywhere here, it is implied that the functions F and G correspond to the angular momentum (1.21), e.g., $F\equiv F_m\equiv F_j$; the index j or m will be often suppressed for brevity. Equations (2.4a) and (2.4b) have been derived by DiVincenzo and Mele[11] for the case $M=0$. In the absence of the potential, $U\equiv 0$, Eqs. (2.4a) and (2.4b) are equivalent to Eqs. (1.19a) and (1.19b).

It is often convenient to represent Eqs. (2.4a) and (2.4b) in a more symmetric form using the eigenvalue (1.21),

$$(F\sqrt{r})'_r-\frac{j}{r}(F\sqrt{r})+(\epsilon+M-U)(G\sqrt{r})=0, \tag{2.5a}$$

$$(G\sqrt{r})'_r+\frac{j}{r}(G\sqrt{r})-(\epsilon-M-U)(F\sqrt{r})=0. \tag{2.5b}$$

Equations. (2.4a), (2.4b), (2.5a), and (2.5b) are valid both for the continuous and for the discrete spectrum (present for $M\neq 0$). In the massless limit $M\to 0$, Eqs. (2.4a), (2.4b), (2.5a), and (2.5b) acquire the following symmetry: For any $U(r)$, if a pair (F,G) is the solution for a given j, then the pair $(G,-F)$ is the corresponding solution for $j\to -j$, i.e.,

$$M=0:\quad F_{-j}=G_j,\quad G_{-j}=-F_j. \tag{2.6}$$

This symmetry is also present for the 3D massless Dirac fermions (Ref. 33, Sec. 38).

The asymmetry between the spinor components associated with the finite Dirac mass M is stressed by rescaling the radial functions in accord with Eq. (1.20),

$$|\epsilon|>M:\begin{array}{c}F\sqrt{r}=\sqrt{\pm(\epsilon+M)}\hat{F},\\ G\sqrt{r}=\pm\sqrt{\pm(\epsilon-M)}\hat{G},\end{array} \tag{2.7}$$

where $\pm$ is sgn ϵ. Then Eqs. (2.5a) and (2.5b) take the form

$$\hat{F}'_r-\frac{j}{r}\hat{F}+p\left[1-\frac{U}{\epsilon+M}\right]\hat{G}=0, \tag{2.8a}$$

$$\hat{G}'_r+\frac{j}{r}\hat{G}-p\left[1-\frac{U}{\epsilon-M}\right]\hat{F}=0. \tag{2.8b}$$

Here, $p=\sqrt{\epsilon^2-M^2}$. The same can be done for the discrete spectrum,

$$|\epsilon|<M:\begin{array}{c}F\sqrt{r}=\sqrt{M+\epsilon}\,\hat{F},\\ G\sqrt{r}=\sqrt{M-\epsilon}\,\hat{G}.\end{array} \tag{2.9}$$

Introducing $\lambda\equiv\sqrt{M^2-\epsilon^2}$, the corresponding equations are

$$\hat{F}'_r-\frac{j}{r}\hat{F}+\lambda\left[1-\frac{U}{M+\epsilon}\right]\hat{G}=0, \tag{2.10a}$$

$$\hat{G}'_r+\frac{j}{r}\hat{G}+\lambda\left[1+\frac{U}{M-\epsilon}\right]\hat{F}=0. \tag{2.10b}$$

Finally, we reduce the system of first-order equations, say Eqs. (2.8a) and (2.8b), to an equivalent second-order equation. The latter can be written either for $\hat{F}$ or for $\hat{G}$ as follows:

$$\hat{F}+\frac{U'\left[\hat{F}-\frac{j}{r}\hat{F}\right]}{\epsilon+M-U}+\left[(\epsilon-U)^2-M^2+\frac{j-j^2}{r^2}\right]\hat{F}=0 \tag{2.11}$$

(the corresponding equation for $\hat{G}$ would have $j\to -j$). Equation (2.11) is reduced to the familiar Schrödinger form

$$\Psi''+2[E-V(r)]\Psi=0,\quad E=p^2/2, \tag{2.12}$$

via the substitution $\hat{F}=\sqrt{\epsilon+M-U}\Psi$. Similar to the 3D case, the potential $V=V_1+V_2$ splits into the Klein-Gordon part V_1 and the part V_2 responsible for the Dirac "spin" effects:

$$V_1=\epsilon U(r)-\frac{1}{2}U^2+\frac{j^2-j}{2r^2}, \tag{2.13}$$

$$V_2=\frac{1}{4}\left[\frac{U''}{\epsilon+M-U}+\frac{3}{2}\left(\frac{U'}{\epsilon+M-U}\right)^2+\frac{2\frac{j}{r}U'}{\epsilon+M-U}\right].$$

It should be clear that the "spin"-orbit coupling coming from the potential V_2 has nothing to do either with the real SU(2) spin of electrons or with having the two Dirac points. Rather, it is a consequence of a two-component spinor structure of the electron wave function due to the existence of the two sublattices in a honeycomb lattice. We also note that the Schrödinger "energy variable" E in Eq. (2.12) has the dimension of [energy]^2, same as that of the potential V. In effect, Eq. (2.12) is a square of the original Dirac problem (2.1); hence, the original potential U alone and even its sign do not have a transparent meaning in problem (2.12).

B. Short-distance behavior: Limitations on the Dirac description

Consider the potential $U(r)$ that at $r\to 0$ is more singular than $1/r$. In this case, for small r, Eqs. (2.4a) and (2.4b) take the form

$$F'_r-UG=0 \text{ and } G'_r+UF=0, \tag{2.14}$$

whose solutions are

$$F = C\sin\left(\int^r Udr + \delta\right), \quad G = C\cos\left(\int^r Udr + \delta\right) \tag{2.15}$$

with constant C and δ. These functions strongly oscillate and have no limit for $r \to 0$. In the nonrelativistic case, this situation would be equivalent to falling into the source of the potential: namely, such a potential allows for infinitely deep-lying bound states.[39] Physically, a sufficiently singular potential in a (massive) relativistic system causes the Dirac vacuum breakdown (the Schwinger effect).[40] Such a singular attractive potential will be responsible for the free emission of electron-hole pairs; if the potential is attractive, electrons would then bind to it, while holes will be pushed to infinity.[33] If the potential is repulsive, it will push away the electrons and bind holes instead.

In the Schrödinger case, falling into the potential center first occurs for the $1/r^2$ singularity.[39] It is not surprising that the Dirac problem is more sensitive to singular behavior at short distances, as it can be roughly thought of as a "square root" of the Schrödinger equation.

As a result of these simple considerations, for both repulsion and attraction, the potentials that are more singular than $1/r$ for $r \to 0$ cannot be correctly considered within the low-energy effective Dirac theory [Eq. (2.1)]. In this case, the exact eigenstates have to be determined on the length scale of the graphene lattice, where the long-wavelength description (2.1) breaks down. Such a situation, where the effect of the lattice cannot be simply incorporated by means of the effective-mass description, is reminiscent of that for the deep-lying impurity levels in the middle of the band gap in a semiconductor, where the effective-mass theory is inapplicable from the outset.

C. Scattering amplitude and cross-section

Below we develop the elastic scattering theory for the 2D Dirac fermions in the presence of the axially symmetric potential $U(r)$. Our goal is to express the scattering amplitude and the cross section in terms of the scattering phase shifts for the spinor spherical waves of the form (1.20).

First, we recall that in the nonrelativistic case, with the incident flux along the $\hat{\mathbf{x}}$ direction, the 2D wave function has the asymptotic form (our notation follows Ref. 39)

$$\Psi \simeq e^{ipx} + \frac{f(\theta)}{\sqrt{-ir}} e^{ipr}, \tag{2.16}$$

where f is the 2D scattering amplitude and the factor $\sqrt{-i} = e^{-i\pi/4}$ is introduced for further convenience. The differential and the total cross sections that have the dimensionality of length are[39]

$$\frac{d\Lambda}{d\theta} = |f(\theta)|^2, \quad \Lambda = \oint |f(\theta)|^2 d\theta. \tag{2.17}$$

(We have denoted the scattering cross section by Λ since the letter σ is commonly reserved for the conductivity.) One way to find the scattering amplitude f is to represent the wave function Ψ in the spherical wave basis, $\Psi = \Sigma_m A_m R_{pm}(r)\Phi_m(\theta)$, and to consider the Schrödinger equation

$$\frac{1}{r}(rR'_{pm})' + \left[p^2 - \frac{m^2}{r^2} - \frac{2MU(r)}{\hbar^2}\right] R_{pm} = 0 \tag{2.18}$$

for each of the radial components R_{pm}. The scattering phase shifts δ_m are then defined by the asymptotic form of the solutions of Eq. (2.18):

$$R_{pm}(r) \simeq \frac{2}{\sqrt{r}} \cos\left(pr - \frac{m\pi}{2} - \frac{\pi}{4} + \delta_m\right). \tag{2.19}$$

Using the decomposition of the plane wave,

$$e^{ipx} = \sum_{m=-\infty}^{\infty} i^m J_m(pr) e^{im\theta}, \tag{2.20}$$

together with definition (2.16), we find

$$A_m = i^m p^{-1/2} e^{i\delta_m} \tag{2.21}$$

and

$$f(\theta) = \frac{1}{i\sqrt{2\pi p}} \sum_{m=-\infty}^{\infty} (S_m - 1) e^{im\theta}, \quad S_m \equiv e^{2i\delta_m}. \tag{2.22}$$

From Eq. (2.22), the total cross section (2.17) follows[41,42]:

$$\Lambda = \frac{4}{p} \sum_{m=-\infty}^{\infty} \sin^2 \delta_m, \tag{2.23}$$

and the momentum-relaxation (transport) cross section

$$\Lambda_{\mathrm{tr}} = \oint d\theta (1 - \cos\theta) |f(\theta)|^2 = \frac{2}{p} \sum_{m=-\infty}^{\infty} \sin^2(\delta_{m+1} - \delta_m). \tag{2.24}$$

With our definition of f, the 2D optical theorem is then

$$\Lambda = \sqrt{8\pi/p}\, \mathrm{Im}\, f(0). \tag{2.25}$$

Turning to the Dirac case with the Hamiltonian (2.1), the asymptotic form for the spinor wave function is

$$\psi = u_{\epsilon,p\hat{\mathbf{x}}} e^{ipx} + \frac{f(\theta)}{\sqrt{-ir}} u_{\epsilon,\mathbf{p}_\theta} e^{ipr}, \tag{2.26}$$

where $\mathbf{p}_\theta = p(\cos\theta, \sin\theta)$ defines the direction of scattering and $u_{\epsilon,\mathbf{p}}$ is the normalized plane wave amplitude (1.9). Since, according to Eq. (1.5), the scattered current

$$\mathbf{J}_{\mathrm{scatt}} = \frac{|f|^2}{r} u^\dagger_{\epsilon,\mathbf{p}_\theta} \boldsymbol{\sigma} u_{\epsilon,\mathbf{p}_\theta} = \frac{|f|^2}{r} \frac{\mathbf{p}_\theta}{\epsilon} \tag{2.27}$$

and the incident current $\mathbf{J}_{\mathrm{in}} = p\hat{\mathbf{x}}/\epsilon$, it follows that the scattering amplitude f is analogous to that in the nonrelativistic case, with the cross section given by Eq. (2.17). Similarly, one defines the scattering phase shifts δ_j via the asymptotic form of the radial wave functions of the spherical spinor (1.18),

$$\psi_j(\mathbf{r}) = \begin{pmatrix} F(r)\Phi_{j-1/2}(\theta) \\ iG(r)\Phi_{j+1/2}(\theta) \end{pmatrix} \tag{2.28}$$

(here we relabeled $\psi_m \to \psi_j$ using Eq. (1.21)). The wave functions F and G are determined by Eqs. (2.4a) and (2.4b), or Eqs. (2.5a) and (2.5b). Their asymptotic behavior should then be compared to that of the free spherical spinor (1.20) with $R_{pm}(r)$ regular at $r=0$,

$$F \simeq \frac{2}{\sqrt{r}}\sqrt{\frac{|\epsilon+M|}{2|\epsilon|}}\cos\left(pr - \frac{j\pi}{2} + \delta_j\right), \tag{2.29a}$$

$$G \simeq \pm\frac{2}{\sqrt{r}}\sqrt{\frac{|\epsilon-M|}{2|\epsilon|}}\sin\left(pr - \frac{j\pi}{2} + \delta_j\right). \tag{2.29b}$$

The spinor wave function (2.26) is represented in basis (1.18) as $\psi=\Sigma_j A_j\psi_j(\mathbf{r})$, where the coefficients A_j, expressed in terms of the phase shifts δ_j introduced in Eq. (2.29), are given by the nonrelativistic Eq. (2.21), $A_j = i^{j-1/2}p^{-1/2}\exp(i\delta_j)$. The scattering amplitude, the cross section, and the optical theorem directly follow, cf. Eqs. (2.22), (2.23), and (2.25), correspondingly,

$$f(\theta) = \frac{1}{i\sqrt{2\pi p}}\sum_{j=\pm1/2,\pm3/2,\ldots,}(S_j-1)e^{i(j-1/2)\theta}, \tag{2.30}$$

where

$$S_j \equiv e^{2i\delta_j}, \tag{2.31}$$

$$\Lambda = \frac{4}{p}\sum_{j=\pm1/2,\pm3/2,\ldots,}\sin^2\delta_j, \tag{2.32}$$

$$\Lambda_{\mathrm{tr}} = \frac{2}{p}\sum_{j=\pm1/2,\pm3/2,\ldots,}\sin^2(\delta_{j+1}-\delta_j). \tag{2.33}$$

Finally, consider the most common massless case, where we derive an important property,

$$M=0: \quad \delta_{-j} = \delta_j. \tag{2.34}$$

For that, we apply symmetry (2.6) to the asymptotic form (2.29) and use Eqs. (1.14a) and (1.14b) [noting that δ_j are defined mod π, since the observable quantities are the S-matrix elements (2.31)]. Property (2.34) ensures that backscattering vanishes in the massless limit:

$$M=0: \quad f(\pi)=0. \tag{2.35}$$

The absence of backscattering is a result of the destructive interference between the time-reversed scattering paths. This happens since the (pseudo)helicity, the eigenvalue of $\hat{\mathbf{p}}\boldsymbol{\sigma}$, is asymptotically conserved during scattering off a potential that does not couple the Dirac points. In other words, the Dirac spin always remains in the direction of the particle's momentum.[43] The time-reversed backscattering paths then acquire phase difference $e^{i\pi}=-1$ that corresponds to the Berry's phase $-i\oint d\tau\psi^\dagger\partial_\tau\psi=\frac{1}{2}\oint d\tau\partial_\tau\theta=\pi$ accumulated while encircling the Dirac point, ψ being the spinors (1.9) with $M=0$.[43]

D. Born approximation

Let us now consider the potential term in the Hamiltonian (2.1) as a perturbation and find the scattering amplitude to the lowest order in U. Following the standard recipe,[39] we write the wave function in the form

$$\psi = \psi^{(0)} + \psi^{(1)}, \tag{2.36}$$

where the unperturbed part $\psi^{(0)}=e^{i\mathbf{pr}}u_{\epsilon;\mathbf{p}}$ is a spinor plane wave (1.9) in the direction of the incident momentum $\mathbf{p}$, and the scattered part obeys the equation

$$[\mathcal{H}_0-\epsilon]\psi^{(1)} = -U\psi^{(0)}. \tag{2.37}$$

The solution of this equation,

$$\psi^{(1)} = -\int d^2\mathbf{r}'G_\epsilon(\mathbf{r}-\mathbf{r}')[-i\boldsymbol{\sigma}\partial_{\mathbf{r}'}+M\sigma_3+\epsilon]U(\mathbf{r}')u_{\epsilon;\mathbf{p}}e^{i\mathbf{pr}'}, \tag{2.38}$$

is found by multiplying both sides by the operator $\mathcal{H}_0+\epsilon$ and evaluating the operator inverse $G_\epsilon=[\mathcal{H}_0^2-(\epsilon+i0\ \mathrm{sgn}\ \epsilon)^2]^{-1}$ in the Fourier space (sgn ϵ selects the retarded or the advanced part, corresponding to the particle and hole sectors):

$$G_\epsilon(\mathbf{r}) = \int\frac{d^2\mathbf{k}}{(2\pi)^2}\frac{e^{i\mathbf{kr}}}{k^2+M^2-(\epsilon+i0\ \mathrm{sgn}\ \epsilon)^2} = \frac{1}{4\pi}(i\pi\ \mathrm{sgn}\ \epsilon)H_0^{(1)}(pr), \tag{2.39}$$

where $p=+\sqrt{\epsilon^2-M^2}$ and

$$H_m^{(1,2)}(x) = J_m(x) \pm iY_m(x) \tag{2.40}$$

are the Hankel's functions of the first and second kind. The asymptotic form of the Green's function (2.39) follows from Eqs. (1.14a) and (1.14b),

$$G_{\pm|\epsilon|}(\mathbf{r}) \simeq \pm\frac{i}{4}\sqrt{\frac{2}{\pi pr}}\,e^{ipr-i\pi/4}. \tag{2.41}$$

We now substitute the asymptotic form (2.41) into Eq. (2.38), applying the standard approximation $|\mathbf{r}-\mathbf{r}'|\approx r-\hat{\mathbf{r}}\cdot\mathbf{r}'$ and $p|\mathbf{r}-\mathbf{r}'|+\mathbf{pr}'\approx pr-\mathbf{qr}'$, where $\mathbf{p}'\equiv p\hat{r}$ is the momentum scattered in the direction of observation and $\mathbf{q}=\mathbf{p}'-\mathbf{p}$ is the momentum transfer. Next, we integrate by parts to switch the derivative

$$e^{-i\mathbf{p}'r'}[-i\boldsymbol{\sigma}\boldsymbol{\partial}_{\mathbf{r}'}+M\sigma_3+\epsilon]e^{i\mathbf{pr}'} \to [\boldsymbol{\sigma}\mathbf{p}'+M\sigma_3+\epsilon]e^{-i\mathbf{qr}'},$$

use $[\boldsymbol{\sigma}\mathbf{p}'+M\sigma_3+\epsilon]u_{\pm|\epsilon|;\mathbf{p}}=\pm pb(\theta)u_{\pm|\epsilon|;\mathbf{p}'}$, and compare the resulting asymptotic form to Eq. (2.26) in order to obtain

$$f^{\mathrm{Born}}(\theta) = -\frac{1}{\hbar v}\sqrt{\frac{p}{8\pi}}\,U_{\mathbf{q}}b(\theta), \tag{2.42}$$

$$b(\theta) = \sqrt{\frac{|\epsilon+Mv^2|}{|\epsilon-Mv^2|}} + e^{-i\theta}\sqrt{\frac{|\epsilon-Mv^2|}{|\epsilon+Mv^2|}}. \tag{2.43}$$

Here, $\theta=\angle(\mathbf{p}',\mathbf{p})$, $q=2p\sin(\theta/2)$, $U_{\mathbf{q}}=\int d\mathbf{r}e^{-i\mathbf{qr}}U(\mathbf{r})$, and the factor (2.43) comes from the spinor structure of the eigenstates (1.9). We restored $\hbar$ and v so that $\mathbf{p}$ are wave

vectors, with $(\hbar vp)^2=\epsilon^2-(Mv^2)^2$, to make it explicit that f has the dimension of $[\text{length}]^{1/2}$.

In the massless limit (pristine graphene), the factor $b(\theta)$ reduces to the familiar expression coming from the Berry phase,[43] yielding

$$f^{\text{Born}}_{M=0}(\theta)=-\frac{1}{\hbar v}\sqrt{\frac{p}{8\pi}}\,U_{\mathbf{q}}(1+e^{-i\theta}). \tag{2.44}$$

For $M=0$, the backscattering is absent in agreement with the general property (2.35).

In the nonrelativistic limit $\epsilon\simeq Mv^2+(\hbar p)^2/2M$, both the spinor part $u_{\mathbf{p}}\to(1\ 0)^T$ and the Berry phase factor $b(\theta)\to 2Mv/\hbar p$ become trivial, yielding[39]

$$f^{\text{Born}}_{\text{nr}}(\theta)=-\frac{M}{\hbar^2\sqrt{2\pi p}}\,U_{\mathbf{q}}. \tag{2.45}$$

E. Analytical properties

Here we derive a few properties of the scattering solutions by considering them as functions of energy ϵ in the complex plane.[39] Consider the $r\to\infty$ asymptotic form of the solution to the radial equations of Sec. II A,

$$F\simeq A(\epsilon)R^+(pr)+B(\epsilon)R^-(pr), \tag{2.46}$$

$p(\epsilon)=\sqrt{(\epsilon-M)(\epsilon+M)}$. Here [cf. Eqs. (1.14)],

$$R^{\pm}(pr)=\sqrt{\frac{\pi p}{2}}e^{\pm i\pi j/2}H^{(1,2)}_m(pr)\simeq\frac{1}{\sqrt{r}}e^{\pm ipr}, \tag{2.47}$$

where $H^{(1,2)}_m$ are the Hankel's functions (2.40). The functions $A(\epsilon)$ and $B(\epsilon)$ become uniquely defined on the physical sheet of the Riemann surface of the square root (Fig. 1) described below. On the physical sheet, the solutions of Eqs. (2.8a) and (2.8b) can be obtained from those of Eq. (2.10) by analytic continuation.

Consider the complex plane of ϵ (Fig. 1) with the branch cuts along the real axis connecting the points $\epsilon=\pm M$ with infinity. The states on the branch cuts correspond to the continuous spectrum, while the real poles in the interval $-M<\epsilon<M$ correspond to the bound states. Define $\sqrt{M-\epsilon}>0$ and $\sqrt{M+\epsilon}>0$ for $-M<\epsilon<M$. Analytic continuation onto $\epsilon>M$ and $\epsilon<-M$ should agree with the standard causality arguments (particles propagate forward in time). Since the time evolution $\sim\theta(t)e^{-i\epsilon_{\mathbf{p}}t}$ of the particle states (Re $\epsilon>M$) is described by the retarded Green's function $G^R(\epsilon)\sim(\epsilon-\epsilon_{\mathbf{p}}+i0)^{-1}$ [here, $\theta(t)$ is a unit step function], the branch cut to the right of M is shifted by the infinitesimal amount $-i0$ below the real axis, Im $\epsilon<0$. The square root $\sqrt{\epsilon-M}$ for $\epsilon>M$ then has to be continued from the upper side of the cut, $\sqrt{\epsilon-M}\to i\sqrt{M-\epsilon}$, as in the Schrödinger case.[39] Conversely, the hole states (Re $\epsilon<-M$) are governed by the advanced propagator $G^A(\epsilon)\sim(\epsilon-\epsilon_{\mathbf{p}}-i0)^{-1}$, such that $\int d\epsilon G^A(\epsilon)e^{-i\epsilon t}\sim\theta(-t)e^{-i\epsilon_{\mathbf{p}}t}$, effectively shifting the other cut above the real axis, Im $\epsilon>0$. The square root $\sqrt{-(\epsilon+M)}$ for $\epsilon<-M$ then has to be continued from the lower side of the cut, $\sqrt{-(\epsilon+M)}\to i\sqrt{\epsilon+M}$. Summarizing,

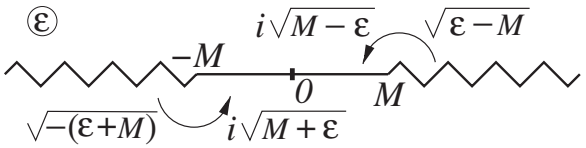

FIG. 1. Analytic continuation in the energy domain.

$$\epsilon>0:\ \sqrt{M-\epsilon}\to-i\sqrt{\epsilon-M}, \tag{2.48a}$$

$$\epsilon<0:\ \sqrt{M+\epsilon}\to-i\sqrt{-(\epsilon+M)}. \tag{2.48b}$$

This determines the sign of the continuation

$$\lambda=\sqrt{M^2-\epsilon^2}\to-ip,\quad p=\sqrt{\epsilon^2-M^2}. \tag{2.48c}$$

Note that the $\pm$ signs in front of the square root in Eq. (2.7) [that agree with those in the free spinor (1.20)] appear naturally as a result of procedure (2.48a), (2.48b), and (2.48c).

The radial functions of the bound states decay for $r\to\infty$. This means that the discrete spectrum corresponds to zeros of the function $B(\epsilon)$ [cf. Eq. (2.47)]. The functions $A(\epsilon)$ and $B(\epsilon)$ are connected to the partial scattering amplitudes (2.31). Indeed, comparing the asymptotic form (2.29a) with Eq. (2.46), we obtain

$$A(\epsilon)/B(\epsilon)=e^{2i\delta_j(\epsilon)-i\pi j}. \tag{2.49}$$

Thus, the amplitude S_j has a pole for any bound state ϵ_b. Following Refs. 33 and 39, we now express the residue of S_j in this pole via the value $A(\epsilon_b)$.

Consider the radial equations (2.5a) and (2.5b). Differentiating them with respect to ϵ, we obtain

$$(\partial_\epsilon F\sqrt{r})'_r-\frac{j}{r}\partial_\epsilon F\sqrt{r}+(\epsilon+M-U)\partial_\epsilon G\sqrt{r}=-G\sqrt{r},$$

$$(\partial_\epsilon G\sqrt{r})'_r+\frac{j}{r}\partial_\epsilon G\sqrt{r}-(\epsilon-M-U)\partial_\epsilon F\sqrt{r}=F\sqrt{r}.$$

Multiply the first one by $-2\sqrt{r}G$, the second one by $2\sqrt{r}F$, then multiply Eq. (2.5a) by $\sqrt{r}G$ and Eq. (2.5b) by $-\sqrt{r}F$, and add up all the four equations. After many terms cancel, what is left can be cast in the following form:

$$\partial_r[r(F\partial_\epsilon G-G\partial_\epsilon F)]=r(F^2+G^2). \tag{2.50}$$

Next, integrate Eq. (2.50) with respect to r from $r=0$ to r, having in mind the limit $r\to\infty$. The right-hand side becomes unity due to normalization, while in the left-hand side we use the asymptotic relation

$$(F\sqrt{r})'_r\simeq-(\epsilon+M)G\sqrt{r} \tag{2.51}$$

that follows from Eq. (2.5a) if one neglects terms with $U(r)$ and j/r. Relation (2.51) allows us to rewrite Eq. (2.50) for $r\to\infty$ in terms of the component F only,

$$(F\sqrt{r})'_r(\partial_\epsilon F\sqrt{r})-(F\sqrt{r})(\partial_\epsilon F\sqrt{r})'_r\simeq\epsilon+M. \tag{2.52}$$

Now consider the asymptotic form (2.46), where we set $A(\epsilon)\simeq A(\epsilon_b)$ and $B(\epsilon)\simeq\beta(\epsilon-\epsilon_b)$, $\beta=[\partial B/\partial\epsilon]_{\epsilon=\epsilon_b}$. Substituting it into Eq. (2.52), we find

$$\beta = -\frac{1}{2A(\epsilon_b)}\sqrt{\frac{M+\epsilon_b}{M-\epsilon_b}}. \tag{2.53}$$

Using Eq. (2.49), we finally obtain the S-matrix residue

$$e^{2i\delta_j(\epsilon)} \simeq -e^{i\pi j}\frac{2[A(\epsilon_b)]^2}{\epsilon-\epsilon_b}\sqrt{\frac{M-\epsilon_b}{M+\epsilon_b}} \tag{2.54}$$

in terms of the coefficient $A(\epsilon_b)$ in the asymptotic form (2.46) of the wave function. We will use the result (2.54) in Sec. IV to normalize the bound state wave functions.

III. LOW-ENERGY SCATTERING

As an application of the developed formalism, consider scattering off a potential $U(r)$ localized within the domain of the size $\sim\ell$ much greater than the graphene lattice constant. For concreteness, take $U(r)=V_0\theta(\ell-r)$. We will be primarily interested in the situation when the range ℓ is small compared to the wavelength, $p\ell<1$.

First note that at large distances, $r>\ell$, where the potential $U(r)$ does not contribute, the radial components of the spinor (1.18) are linear combinations of the corresponding free solutions (1.20),

$$F|_{r>\ell} = C\sqrt{|\epsilon+M|}\{J_m(pr)\cos\delta_j - Y_m(pr)\sin\delta_j\}, \tag{3.1a}$$

$$G|_{r>\ell} = \pm C\sqrt{|\epsilon-M|}\{J_{m+1}(pr)\cos\delta_j - Y_{m+1}(pr)\sin\delta_j\}, \tag{3.1b}$$

where $j=m+\frac{1}{2}$ and $C=\sqrt{\pi p/|\epsilon|}$.

For $r<\ell$, the regular at $r=0$ solutions take the form

$$F|_{r<\ell} = \tilde{C}\sqrt{|\tilde{\epsilon}+M|}J_m(\tilde{p}r), \tag{3.2a}$$

$$G|_{r<\ell} = (\mathrm{sgn}\,\tilde{\epsilon})\tilde{C}\sqrt{|\tilde{\epsilon}-M|}J_{m+1}(\tilde{p}r). \tag{3.2b}$$

Here, we introduced $\tilde{\epsilon}=\epsilon-V_0$ and $\tilde{p}\equiv\sqrt{\tilde{\epsilon}^2-M^2}$. Solutions (3.2a) and (3.2b) are written for $|\tilde{\epsilon}|>M$. For $|\tilde{\epsilon}|<M$, $\tilde{p}\to i\tilde{\lambda}$ (cf. Sec. II E, $\epsilon\to\tilde{\epsilon}$), their counterparts read

$$F|_{r<\ell} = \tilde{C}'\sqrt{M+\tilde{\epsilon}}\,I_m(\tilde{\lambda}r), \tag{3.2c}$$

$$G|_{r<\ell} = -\tilde{C}'\sqrt{M-\tilde{\epsilon}}\,I_{m+1}(\tilde{\lambda}r), \tag{3.2d}$$

where $I_m(x)=i^{-m}J_m(ix)$ is the modified Bessel function of the first kind and $\tilde{C}$ and $\tilde{C}'$ are constants that can be chosen real.

Both spinor components must be continuous at $r=\ell$. This translates into the following matching condition:

$$\left.\frac{F}{G}\right|_{r<\ell} = \left.\frac{F}{G}\right|_{r>\ell}, \tag{3.3}$$

yielding (for $|\tilde{\epsilon}|>M$)

$$\tilde{\zeta}\frac{J_m(\tilde{p}\ell)}{J_{m+1}(\tilde{p}\ell)} = \zeta\frac{J_m(p\ell)-Y_m(p\ell)\tan\delta_j}{J_{m+1}(p\ell)-Y_{m+1}(p\ell)\tan\delta_j}, \tag{3.4}$$

where

$$\zeta = (\mathrm{sgn}\,\epsilon)\sqrt{\left|\frac{\epsilon+M}{\epsilon-M}\right|}, \quad \tilde{\zeta} = (\mathrm{sgn}\,\tilde{\epsilon})\sqrt{\left|\frac{\tilde{\epsilon}+M}{\tilde{\epsilon}-M}\right|}. \tag{3.5}$$

For $|\tilde{\epsilon}|<M$, $\tilde{\zeta}\to -i\sqrt{\frac{M+\tilde{\epsilon}}{M-\tilde{\epsilon}}}$ (cf. Sec. II E), and the left-hand side of Eq. (3.4) is analytically continued to $-\sqrt{\frac{M+\tilde{\epsilon}}{M-\tilde{\epsilon}}}I_m(\tilde{\lambda}\ell)/I_{m+1}(\tilde{\lambda}\ell)$, in accord with what one gets by applying condition (3.3) directly to Eqs. (3.2c) and (3.2d). Hence, we will work with Eq. (3.4) keeping in mind this analytic continuation for $|\tilde{\epsilon}|<M$.

As a result, from Eq. (3.4), we find [cf. Eq. (2.40)]

$$S_j - 1 = 2\frac{\zeta J_{m+1}(\tilde{p}\ell)J_m(p\ell) - \tilde{\zeta}J_m(\tilde{p}\ell)J_{m+1}(p\ell)}{\tilde{\zeta}J_m(\tilde{p}\ell)H^{(1)}_{m+1}(p\ell) - \zeta J_{m+1}(\tilde{p}\ell)H^{(1)}_m(p\ell)}. \tag{3.6}$$

For the massless case [$\zeta,\tilde{\zeta}\to\pm$], Eq. (3.6) has been first obtained in Ref. 26 (see also Ref. 27).

For short-ranged scatterers, $p\ell\ll 1$, the $j=\pm\frac{1}{2}$ channels provide the main contribution. Indeed, for $m\neq 0,-1$, the corresponding S_j-1 are small as powers of $p\ell$; this can be seen from the short-distance behavior (1.15). The scattering amplitude can be thus approximated by taking into account only the $j=\pm\frac{1}{2}$ channels,

$$f(\theta) \simeq \sqrt{\frac{\pi}{2p}}\left[\frac{1}{\frac{\tilde{\zeta}}{\zeta}\frac{J_0(\tilde{p}\ell)}{p\ell J_1(\tilde{p}\ell)} - \ln\frac{2i}{\gamma_E p\ell}} + \frac{e^{-i\theta}}{\frac{\tilde{\zeta}}{\zeta}\frac{J_0(\tilde{p}\ell)}{p\ell J_1(\tilde{p}\ell)} - \ln\frac{2i}{\gamma_E p\ell}}\right]. \tag{3.7}$$

Here, we utilized the asymptotic behavior of the Hankel's functions (2.40),

$$H^{(1)}_0(x) \simeq -\frac{2i}{\pi}\ln\frac{2i}{\gamma_E x}, \quad H^{(1)}_1(x) \simeq \frac{2}{i\pi x}. \tag{3.8}$$

In the massless limit, relevant for scattering off short-ranged impurities in pristine graphene, the $H^{(1)}_1(p\ell)$ contribution dominates, and the amplitude (3.7) is small as $f\sim p^{-1/2}\times p\ell(1+e^{-i\theta})$,[26] resulting in negligible scattering away from resonance [$J_0(\tilde{p}\ell)\neq 0$]. The angular distribution of the scattered particles has a distinctive $\cos^2(\theta/2)$ dependence that comes from the spinor structure of eigenstates (1.9) and agrees with the general property (2.35).

In the opposite, nonrelativistic limit, $\zeta\gg\tilde{\zeta}$, the first term ($m=0$ channel) determines the amplitude (3.7), where now only the logarithmic term coming from $H^{(1)}_0(p\ell)$ can be kept in the denominator.[39]

IV. COULOMB SCATTERING

A. Short-distance behavior: Critical field strength

The analysis of Sec. II B shows that the low-energy Dirac theory is inconsistent with singular potentials $U\sim r^{-s}$, $s>1$. Hence, it is clear that the Coulomb potential

$$U(r)=-\hbar v\frac{\alpha}{r} \tag{4.1}$$

is a borderline case which should be studied with care: Any slightly more singular potential at $r\to 0$ would cause the Dirac vacuum breakdown. Below, we consider the potential (4.1) where the strength α can be both positive (attraction) and negative (repulsion).

Suppose for now that the effective impurity strength α is sufficiently small and consider Eqs. (2.5). Taking the short-distance behavior of the radial wave function as $F\sqrt{r}\sim r^{\gamma}$ and $G\sqrt{r}\sim r^{\gamma}$ and neglecting the nonsingular terms as $r\to 0$, we obtain

$$\gamma=\sqrt{j^2-\alpha^2},\quad j=\pm\tfrac{1}{2},\pm\tfrac{3}{2},\ldots\ . \tag{4.2}$$

The theory [Eqs. (2.1) and (4.1)] is then consistent when $|\alpha|<|j|$ for any possible j, i.e., under the condition

$$|\alpha|<\tfrac{1}{2}. \tag{4.3}$$

For imaginary γ, i.e., when $|\alpha|$ exceeds $|j|$, the eigenstates F and G oscillate and have no well-defined limit as $r\to 0$, which corresponds to the Dirac vacuum breakdown in the same sense as in the discussion of Sec. II B. Such an upper bound on the potential strength is similar to that in the nonrelativistic collapse in the $1/r^2$ potential.[39]

Condition (4.3) appears to be even more restrictive than that in 3D, where the Dirac theory with a pointlike Coulomb potential source is consistent for $|\alpha|<1$.[33] The problem of what happens when $\alpha>1$ in 3D has been the subject of intense theoretical investigation.[35–38] Classically, this instability corresponds to falling of a K-shell electron into the potential center. On a quantum level, the Dirac vacuum breaks down by a sufficiently strong Coulomb center with Z above a certain value Z_c by creating electron-positron pairs; an electron then binds to the nucleus while a positron flies off to infinity. The major difficulty is that the $Z>Z_c$ problem requires ultraviolet regularization, such as introducing the finite size of the nucleus.[35] However, due to very small value of the fine structure constant $e^2/\hbar c=1/137$, the consequences of this restriction never materialized in QED for the K-electrons in heavy atoms, as $Ze^2/\hbar c<1$ for all the known elements in the periodic table, $Z\lesssim 110$.

In a physically relevant case when the field (4.1) is due to a Coulomb impurity in the vicinity of the graphene sheet, the bare potential strength

$$\alpha_0=\frac{Ze_*^2}{\hbar v},\quad e_*^2=\frac{2e^2}{\varepsilon+1}. \tag{4.4}$$

Here, Z is the impurity valence, e is the unit charge, and ε is the dielectric constant of a substrate. The vacuum value $\alpha_0|_{Z=1,\varepsilon=1}\approx 2.2$ for $v=1\times 10^6$ m/s, while for the SiO_2 substrate, $\alpha_0|_{Z=1,\varepsilon=3.9}\approx 0.9$.

Electron-electron interactions result in screening which generally changes the shape of the potential. This is what usually happens in a semiconductor with a parabolic band, where the Coulomb potential is cut off on the screening length scale. In graphene, due to the semimetallic electron dispersion, the screening is unusual. In particular, for massless Dirac fermions at half filling, the linear [random-phase approximation (RPA)] screening is scale invariant[15,44]: it preserves the shape of the potential and simply reduces the impurity strength,

$$\alpha_0\to\alpha=\alpha_0/\varepsilon_{\mathrm{RPA}}, \tag{4.5}$$

by the factor

$$\varepsilon_{\mathrm{RPA}}=1+\frac{q}{4\hbar v}\frac{2\pi e_*^2}{q}=1+\frac{\pi}{2}\frac{e_*^2}{\hbar v}. \tag{4.6}$$

Taking literally, the linear screening yields the reduction by the factor $\varepsilon_{\mathrm{RPA}}|_{\varepsilon=3.9}\approx 2.4$ for an impurity strength in the presence of the SiO_2 substrate, $\alpha|_{Z=1,\varepsilon=3.9}\approx 0.4$.

As one can readily see, due to the threshold (4.3), and a sufficiently small Fermi velocity $v\approx c/300$, the situation in graphene is more complex than that in QED. For sufficiently large values of α, especially for multivalent impurities, the nonlinear screening should be applied instead of the linear (RPA) response, as the latter formally applies only for $e_*^2/\hbar v\ll 1$. In particular, a practically important question is whether the threshold (4.3) can at all be determined within the linear screening framework (4.6), i.e., whether it applies to the screened value (4.5). Strictly speaking, near the threshold, where the bare $\alpha_0\sim 1$, the lattice-scale physics starts playing a role, while the RPA dielectric constant applies in the limit of large distances and weak perturbations. The definition of the threshold as $|\alpha_0|/\varepsilon_{\mathrm{RPA}}<1/2$ may probably be used only as an upper estimate of the threshold value.

An even more interesting problem is the screening in the massive case. The linear screening, formally valid for $e_*^2/\hbar v\ll 1$, is cut off beyond (reduced) Compton wavelength $\lambda_C=\hbar/Mv$; hence, the shape of the potential becomes more complex. For sufficiently weak interactions, $e_*^2/\hbar v\ll 1$, one may argue that the screening can be neglected, $\alpha\simeq\alpha_0$, at low energies (e.g., for describing the bound states), since the corresponding Bohr radius $a_B=\lambda_C/(e_*^2/\hbar v)\gg\lambda_C$. Taking into account corrections in $e_*^2/\hbar v$ would then amount to the "fine structure" of the "atomic levels" associated with the impurity. On the other hand, for $e_*^2/\hbar v\sim 1$, the Bohr radius and the Compton wavelength coincide; such a strongly interacting relativistic Dirac atom will have deep-lying bound states. For sufficiently strong potential, these states will reach the hole continuum (critical impurity), resulting in the vacuum breakdown. In general, this strong-coupling problem, that requires investigation of the supercritical region, involves many body treatment that is beyond the scope of this work. In what follows, we will assume that condition (4.3) holds for the effective value of impurity strength α and consider only the subcritical regime.

B. Discrete spectrum, $|\epsilon|<M$

Similar to the 3D case,[33] we look for the solutions of Eqs. (2.5a) and (2.5b) in the form ($\hbar=v=1$)

$$F=\sqrt{M+\epsilon}\,e^{-\rho/2}\rho^{\gamma-1/2}\tilde{F}(\rho), \tag{4.7a}$$

$$G=\sqrt{M-\epsilon}\,e^{-\rho/2}\rho^{\gamma-1/2}\tilde{G}(\rho). \tag{4.7b}$$

Here, $\rho=2\lambda r$, and $\lambda=\sqrt{M^2-\epsilon^2}$. After substituting the functions (4.7a) and (4.7b) into Eqs. (2.4a) and (2.4b), we obtain the equations for $\tilde{F}$ and $\tilde{G}$:

$$\rho\tilde{F}_\rho'+(\gamma-j)\tilde{F}-\frac{\rho}{2}(\tilde{F}-\tilde{G})+\frac{\lambda\alpha}{M+\epsilon}\tilde{G}=0, \tag{4.8a}$$

$$\rho\tilde{G}_\rho'+(\gamma+j)\tilde{G}+\frac{\rho}{2}(\tilde{F}-\tilde{G})-\frac{\lambda\alpha}{M-\epsilon}\tilde{F}=0. \tag{4.8b}$$

Representing

$$\tilde{F}=Q_1+Q_2 \quad \text{and } \tilde{G}=Q_1-Q_2, \tag{4.9}$$

we find

$$\rho Q_1'+\left(\gamma-\frac{\alpha\epsilon}{\lambda}\right)Q_1-\left(j+\frac{M\alpha}{\lambda}\right)Q_2=0, \tag{4.10a}$$

$$\rho Q_2'+\left(\gamma-\rho+\frac{\alpha\epsilon}{\lambda}\right)Q_2-\left(j-\frac{M\alpha}{\lambda}\right)Q_1=0, \tag{4.10b}$$

from which the equations for Q_1 and Q_2 are

$$\rho Q_1''+(1+2\gamma-\rho)Q_1'-\left(\gamma-\frac{\alpha\epsilon}{\lambda}\right)Q_1=0, \tag{4.11a}$$

$$\rho Q_2''+(1+2\gamma-\rho)Q_2'-\left(1+\gamma-\frac{\alpha\epsilon}{\lambda}\right)Q_2=0. \tag{4.11b}$$

To derive Eq. (4.11), we used the identity

$$j^2-M^2\alpha^2/\lambda^2=\gamma^2-\alpha^2\epsilon^2/\lambda^2. \tag{4.12}$$

Equations (4.11a) and (4.11b) are of the Kummer form,

$$z\mathcal{F}''+(c-z)\mathcal{F}'-a\mathcal{F}=0, \tag{4.13}$$

where $\mathcal{F}$ is the confluent hypergeometric function

$$\mathcal{F}(a,c;z)=1+\frac{a}{c}\frac{z}{1!}+\frac{a(a+1)}{c(c+1)}\frac{z^2}{2!}+\cdots. \tag{4.14}$$

Thus, the solutions of Eqs. (4.11a) and (4.11b) are

$$Q_1=C_1\mathcal{F}(\gamma-\alpha\epsilon/\lambda,1+2\gamma;\rho), \tag{4.15a}$$

$$Q_2=C_2\mathcal{F}(1+\gamma-\alpha\epsilon/\lambda,1+2\gamma;\rho). \tag{4.15b}$$

Using $\mathcal{F}(a,c;0)=1$ and Eqs. (4.10a) and (4.10b), we find the ratio

$$c_{12}\equiv\frac{C_2}{C_1}=\frac{\gamma-\alpha\epsilon/\lambda}{j+M\alpha/\lambda} \tag{4.16}$$

and the wave functions of the bound states,

$$F=\sqrt{M+\epsilon}\,e^{-\rho/2}\rho^{\gamma-1/2}C_1\{\mathcal{F}(\gamma-\alpha\epsilon/\lambda,1+2\gamma;\rho)+c_{12}\mathcal{F}(1+\gamma-\alpha\epsilon/\lambda,1+2\gamma;\rho)\}, \tag{4.17a}$$

$$G=\sqrt{M-\epsilon}\,e^{-\rho/2}\rho^{\gamma-1/2}C_1\{\mathcal{F}(\gamma-\alpha\epsilon/\lambda,1+2\gamma;\rho)-c_{12}\mathcal{F}(1+\gamma-\alpha\epsilon/\lambda,1+2\gamma;\rho)\}, \tag{4.17b}$$

where C_1 is the overall normalization factor.

Bound states occur when the functions $\mathcal{F}$ reduce to polynomials, i.e., when

$$\gamma(j)-\frac{\alpha\epsilon_{n,j}}{\lambda(\epsilon_{n,j})}=-n, \quad \begin{cases} n=0,1,2,\ldots, & \text{for } j>0 \\ n=1,2,3,\ldots, & \text{for } j<0. \end{cases} \tag{4.18}$$

From Eq. (4.18) the bound state energies follow[34]:

$$\epsilon_{n,j}=\frac{M\,\mathrm{sgn}\,\alpha}{\sqrt{1+\dfrac{\alpha^2}{(n+\gamma)^2}}}, \quad \gamma(j)=\sqrt{j^2-\alpha^2}. \tag{4.19}$$

The bound states are doubly degenerate, $\epsilon_{n,j}=\epsilon_{n,-j}$.

The overall normalization factor C_1 can be found by comparing the $r\to\infty$ asymptotic behavior of the function (4.17a) (where the leading contribution comes only from the first term), with Eq. (4.34) that will be obtained below. The asymptotic behavior of Eq. (4.17a),

$$F\simeq(-)^nC_1\frac{\Gamma(1+2\gamma)\sqrt{M+\epsilon}}{\Gamma(1+2\gamma+n)}(2\lambda r)^{n+\gamma-1/2}e^{-\lambda r},$$

is found using the formula

$$\mathcal{F}(a,c;z)=\frac{\Gamma(c)}{\Gamma(c-a)}(-z)^{-a}\mathcal{G}(a,a-c+1,-z)+\frac{\Gamma(c)}{\Gamma(a)}e^zz^{a-c}\mathcal{G}(c-a,1-a,z), \tag{4.20}$$

$$\mathcal{G}(a,c;z)=1+\frac{ac}{1!\times z}+\frac{a(a+1)c(c+1)}{2!\times z^2}+\cdots \tag{4.21}$$

[Ref. 39, Eq. (d.14)]. As a result, the wave functions for the bound states (the upper sign corresponds to F and the lower one to G; $\epsilon\equiv\epsilon_{n,j}$) are

$$\begin{Bmatrix} F \\ G \end{Bmatrix}=\frac{(-)^n\lambda^{3/2}}{M\Gamma(1+2\gamma)}\sqrt{\frac{\Gamma(1+2\gamma+n)(M\pm\epsilon)}{(j+M\alpha/\lambda)\alpha n!}}\times e^{-\lambda r}(2\lambda r)^{\gamma-1/2}\{(j+M\alpha/\lambda)\mathcal{F}(-n,1+2\gamma;2\lambda r)\mp n\mathcal{F}(1-n,1+2\gamma;2\lambda r)\}. \tag{4.22}$$

The functions (4.22) are normalized to $\int_0^\infty rdr(F^2+G^2)=1$.

The size $l_{n,j}$ of the bound state wave functions (4.22) is controlled by the parameter $\lambda=\lambda(\epsilon_{n,j})$, as

$$l(\epsilon_{n,j}) \equiv \frac{1}{\lambda(\epsilon_{n,j})} = \frac{\sqrt{(n+\gamma)^2+\alpha^2}}{(Mv/\hbar)|\alpha|} \equiv \sqrt{(n+\gamma)^2+\alpha^2}\, a_B/Z, \quad a_B = \frac{\hbar^2}{Me_*^2}, \tag{4.23}$$

scaling with the "Bohr radius" a_B that is a ratio of the reduced Compton wavelength $\hbar/Mv$ and the effective fine structure constant $e_*^2/\hbar v$ (note again that we assume weak coupling $e_*^2/\hbar v \ll 1$).

C. Continuous spectrum, $|\epsilon|>M$

The simplest way to obtain the continuous spectrum solutions in the problem [Eqs. (2.1) and (4.1)] is to analytically continue solutions (4.17a) and (4.17b) according to the procedure (2.48a), (2.48b), and (2.48c). This yields $\rho \to -2ipr$, and the ratio (4.16) becomes

$$c_{12} \to e^{-2i\xi_j} = \frac{\gamma - i\alpha_\epsilon}{j + iM\alpha/p}, \quad \alpha_\epsilon \equiv \frac{\alpha\epsilon}{p}. \tag{4.24}$$

The phase ξ_j is real due to the identity (4.12).

Consider now the $|\epsilon|<M$ solutions (4.17). The analytic continuation $|\epsilon|<M \to |\epsilon|>M$ to the continuous spectrum, using Eqs. (2.48a), (2.48b), (2.48c), and (4.24), yields

$$F = \sqrt{|\epsilon+M|}e^{ipr}r^{\gamma-1/2}C_1'\{e^{i\xi}\mathcal{F}(\gamma - i\alpha_\epsilon, 1+2\gamma; -2ipr) + e^{-i\xi}\mathcal{F}(1+\gamma - i\alpha_\epsilon, 1+2\gamma; -2ipr)\}, \tag{4.25a}$$

$$G = \mp i\sqrt{|\epsilon-M|}e^{ipr}r^{\gamma-1/2}C_1'\{e^{i\xi}\mathcal{F}(\gamma - i\alpha_\epsilon, 1+2\gamma; -2ipr) - e^{-i\xi}\mathcal{F}(1+\gamma - i\alpha_\epsilon, 1+2\gamma; -2ipr)\}, \tag{4.25b}$$

where C_1' is some new overall normalization factor that has to be found by matching the asymptotic behavior of the solutions (4.25a) and (4.25b) with Eq. (2.29). For that, we first consider the asymptotic behavior of the second terms in Eqs. (4.25a) and (4.25b). Using the identity [see, e.g., Ref. 39, Eq. (d.10)]

$$\mathcal{F}(a,c;z) = e^z\mathcal{F}(c-a,c,-z), \tag{4.26}$$

we transform

$$\mathcal{F}(1+\gamma - i\alpha_\epsilon, 1+2\gamma; -2ipr) = e^{-2ipr}[\mathcal{F}(\gamma - i\alpha_\epsilon, 1+2\gamma; -2ipr)]^*. \tag{4.27}$$

As a result, we obtain the normalized eigenstates for the continuous spectrum,

$$F = \frac{2}{\sqrt{r}}\sqrt{\frac{|\epsilon+M|}{2|\epsilon|}}\frac{|\Gamma(1+\gamma+i\alpha_\epsilon)|}{\Gamma(1+2\gamma)} \times e^{\pi\alpha_\epsilon/2}(2pr)^\gamma \mathrm{Re}\{e^{ipr+i\xi}\mathcal{F}(\gamma - i\alpha_\epsilon, 1+2\gamma; -2ipr)\}, \tag{4.28a}$$

$$G = \pm\frac{2}{\sqrt{r}}\sqrt{\frac{|\epsilon-M|}{2|\epsilon|}}\frac{|\Gamma(1+\gamma+i\alpha_\epsilon)|}{\Gamma(1+2\gamma)} \times e^{\pi\alpha_\epsilon/2}(2pr)^\gamma \mathrm{Im}\{e^{ipr+i\xi}\mathcal{F}(\gamma - i\alpha_\epsilon, 1+2\gamma; -2ipr)\}. \tag{4.28b}$$

Note that for $\epsilon<-M$, the analytic continuation (2.48b) produces an extra minus sign for G (here, $\pm=\mathrm{sgn}\,\epsilon$), as expected from the asymptotic behavior (2.29). One can prove that solutions (4.28a) and (4.28b) are correctly normalized by using formula (4.20). The asymptotic $pr\to\infty$ behavior of the normalized solutions (4.28),

$$F \simeq \frac{2}{\sqrt{r}}\sqrt{\frac{|\epsilon+M|}{2|\epsilon|}}\cos(pr - j\pi/2 + \alpha_\epsilon \ln 2pr + \delta_j),$$

$$G \simeq \pm\frac{2}{\sqrt{r}}\sqrt{\frac{|\epsilon-M|}{2|\epsilon|}}\sin(pr - j\pi/2 + \alpha_\epsilon \ln 2pr + \delta_j), \tag{4.29}$$

deviates from that of Eqs. (2.29a) and (2.29b) by the familiar logarithmically divergent Coulomb phase $\ln(2pr)$, ubiquitous in both the nonrelativistic[39,41,42] and the relativistic[33] cases. The scattering phases are then

$$\delta_j = \xi_j + \frac{\pi}{2}(j-\gamma) - \arg\Gamma\left(1+\gamma+\frac{i\alpha\epsilon}{p}\right), \tag{4.30}$$

with the corresponding S-matrix elements (2.22)

$$S_j = e^{2i\delta_j} = \frac{j+iM\alpha/p}{\gamma - i\alpha\epsilon/p}\frac{\Gamma(1+\gamma - i\alpha\epsilon/p)}{\Gamma(1+\gamma+i\alpha\epsilon/p)}e^{i\pi(j-\gamma)}. \tag{4.31}$$

As expected, the poles of S_j determined by the gamma function in the numerator of Eq. (4.31) for $1+\gamma - i\alpha\epsilon/p = 1-n$, $n=1,2,\ldots$, as well as by $\gamma - i\alpha\epsilon/p = 0$ for $j>0$, which occur for the imaginary $p=i\lambda$, give the corresponding bound states (4.19). The residues at these poles are

$$S_j \simeq (-)^{n+1}\frac{\lambda^3(j+M\alpha/\lambda)e^{i\pi(j-\gamma)}}{\alpha M^2 n!\Gamma(1+2\gamma+n)(\epsilon-\epsilon_{n,j})}. \tag{4.32}$$

We now derive the asymptotic form of the discrete spectrum wave functions based on relation (2.54) between the S-matrix residue and the coefficient A in the asymptotic form of the wave function (2.46). In the case of the Coulomb scattering, the coefficient A will itself depend on r due to the logarithmically divergent Coulomb phase. In particular, the left-hand side of Eq. (2.54) should be corrected by the factor $e^{2i\alpha_\epsilon \ln 2pr} \to (-)^n e^{i\pi\gamma}(2\lambda r)^{2(n+\gamma)}$. As a result, near the pole,

$$S_j e^{2i\alpha_\epsilon \ln 2pr} \to -e^{i\pi j}\frac{\lambda^3(j+M\alpha/\lambda)(2\lambda r)^{2(n+\gamma)}}{\alpha M^2 n!\Gamma(1+2\gamma+n)(\epsilon-\epsilon_{n,j})}, \tag{4.33}$$

which, in turn, equals the right-hand side of Eq. (2.54). Thus, we obtain the asymptotic form

$$F \simeq \frac{A(r)}{\sqrt{r}}e^{-\lambda r}, \quad r\to\infty,$$

$$A(r) = \frac{\hbar\lambda}{Mv}\sqrt{\frac{(Mv^2+\epsilon)(j+\alpha Mv/\hbar\lambda)}{2\hbar v\,\alpha n!\Gamma(1+2\gamma+n)}}(2\lambda r)^{n+\gamma}. \tag{4.34}$$

Here, we restored $\hbar$ and v, with $\hbar\lambda/v=\sqrt{M^2-\epsilon^2}$, so that the dimension of F is explicitly 1/[length]. Note also that $|j| < \alpha Mv/\hbar\lambda(\epsilon_{n,j})$, so that $A(r)$ is always real.

1. Nonrelativistic limit (parabolic band)

The nonrelativistic limit occurs when the "nonrelativistic velocity" $v_{\rm nr}$ of the particle is much smaller than the graphene Fermi velocity ("speed of light" v) (which we write here explicitly),

$$v_{\rm nr} \ll v, \quad v_{\rm nr} \equiv \frac{\hbar p}{M}, \quad \epsilon_{\rm nr} \equiv \epsilon - Mv^2 \simeq \frac{(\hbar p)^2}{2M} \ll Mv^2. \tag{4.35}$$

In the limit $v\to\infty$, the fine structure constant $\alpha\to 0$, whereas the "nonrelativistic fine structure constant"

$$\alpha_{\rm nr} \equiv \frac{Ze_*^2}{\hbar v_{\rm nr}} = \frac{v}{v_{\rm nr}}\alpha \tag{4.36}$$

remains finite and determines the Coulomb interaction strength. In this case,

$$\alpha\frac{\epsilon}{\hbar pv} \to \alpha_{\rm nr}, \quad \alpha\frac{Mv}{\hbar p} \to \alpha_{\rm nr}, \quad \gamma \to |j| = |m| + \frac{1}{2}\text{sign}\, j, \tag{4.37}$$

and using $e^{i\pi(j-|j|)}=\text{sgn}\, j$ and $\Gamma(1+z)=z\Gamma(z)$, we obtain

$$S_m^{\rm nr} = e^{2i\delta_m^{\rm nr}} = \frac{\Gamma\left(|m|+\frac{1}{2}-i\alpha_{\rm nr}\right)}{\Gamma\left(|m|+\frac{1}{2}+i\alpha_{\rm nr}\right)}. \tag{4.38}$$

It is instructive to show by a direct calculation, given below, that the phases (4.38) agree with the asymptotic behavior of the radial Schrödinger wave function $R_m(r)$ of the corresponding nonrelativistic Coulomb problem. The radial equation in the presence of the Coulomb potential $U(r)\equiv -Ze_*^2/r$ reads

$$-\frac{1}{r}\frac{d}{dr}\left(r\frac{d}{dr}R\right) + \frac{m^2}{r^2}R - \frac{2MZe_*^2}{\hbar^2 r}R = \frac{2M\epsilon_{\rm nr}}{\hbar^2}R. \tag{4.39}$$

We begin with the bound states. After the substitution

$$R = \rho^{|m|}e^{-\rho/2}Q(\rho), \quad \rho = 2\lambda_{\rm nr}r, \quad \hbar\lambda_{\rm nr} = \sqrt{-2M\epsilon_{\rm nr}}, \tag{4.40}$$

the problem is reduced to the Kummer equation

$$\rho Q'' + (2|m|+1-\rho)Q' - \left(|m|+\tfrac{1}{2}-\tilde\alpha\right)Q = 0, \tag{4.41}$$

where

$$\tilde\alpha = \tilde\alpha(\epsilon_{\rm nr}) = \frac{Z}{a_B\lambda_{\rm nr}} \equiv \frac{MZe_*^2}{\hbar^2\lambda_{\rm nr}}. \tag{4.42}$$

Its solutions

$$R = C_{\rm nr}(2\lambda_{\rm nr}r)^{|m|}e^{-\lambda_{\rm nr}r}\mathcal{F}(-\tilde n, 2|m|+1; 2\lambda_{\rm nr}r),$$

$$-\tilde n \equiv |m| + \tfrac{1}{2} - \tilde\alpha(\epsilon_{\rm nr}),$$

$$C_{\rm nr} = (-)^{\tilde n}\frac{\sqrt{2}\lambda_{\rm nr}\sqrt{(2|m|+\tilde n)!}}{(2|m|)!\sqrt{\tilde n!\left(\tilde n+|m|+\frac{1}{2}\right)}} \tag{4.43}$$

become normalizable, $\int_0^\infty rdrR^2(r)=1$, with

$$\mathcal{F}(-\tilde n, 2|m|+1; 2\lambda_{\rm nr}r) = \frac{(2|m|)!\tilde n!}{[(\tilde n+2|m|)!]^2}L_{\tilde n+2|m|}^{2|m|}(2\lambda_{\rm nr}r) \tag{4.44}$$

given by the associated Laguerre polynomials, when $\tilde n = 0,1,2,\ldots$, yielding the nonrelativistic spectrum[45]

$$\epsilon_{\rm nr} = -\frac{Z^2Me_*^4}{2\hbar^2}\frac{1}{\left(\tilde n+|m|+\frac{1}{2}\right)^2}, \quad \tilde n = 0,1,2,\ldots, \tag{4.45}$$

in agreement with the corresponding limit of the bound states (4.19). [Taking into account the discarded terms $\sim e_*^2/\hbar v$ would correspond to the fine structure of the energy levels (4.45).]

The normalization coefficient $C_{\rm nr}$ for the bound state solutions (4.43) is found, as above, via comparing their $r\to\infty$ asymptotic behavior with the nonrelativistic limit of Eq. (4.34),

$$R_{r\to\infty} \simeq \frac{\sqrt{2}\lambda_{\rm nr}(2\lambda_{\rm nr}r)^{\tilde n+|m|}}{\sqrt{\tilde n!(\tilde n+2|m|)!\left(\tilde n+|m|+\frac{1}{2}\right)}}e^{-\lambda_{\rm nr}r}. \tag{4.46}$$

While obtaining Eq. (4.46), we identified [cf. Eq. (4.18)]

$$\frac{\alpha Mv}{\hbar\lambda}, \frac{\alpha\epsilon_{n,j}}{\hbar v\lambda} \to \tilde\alpha = n + |j| \equiv \tilde n + |m| + \frac{1}{2}. \tag{4.47}$$

The analytic continuation of solutions (4.43) via $\lambda_{\rm nr}\to -ip$, $\tilde\alpha\to i\alpha_{\rm nr}$, and subsequent asymptotic expansion using both terms in formula (4.20), yields

$$R_m \simeq \frac{2}{\sqrt{r}}\cos\left(pr + \alpha_{\rm nr}\ln 2pr + \delta_m^{\rm nr} - \frac{m\pi}{2} - \frac{\pi}{4}\right), \tag{4.48}$$

where the scattering phase shifts (defined mod π)

$$\delta_m^{\rm nr} = -\arg\Gamma\left(|m|+\tfrac{1}{2}+i\alpha_{\rm nr}\right) \tag{4.49}$$

correspond to the S-matrix elements (4.38).

2. Ultrarelativistic limit (graphene)

In the ultrarelativistic limit $|\epsilon| \gg Mv^2$ relevant for pristine graphene monolayer [$M=0$],

$$\alpha_\epsilon = \alpha\epsilon/pv \to \alpha\,\text{sgn}\,\epsilon. \tag{4.50}$$

In this case, similar to the 3D Dirac fermions,[33] the S-matrix elements (4.31) become independent of the absolute value of energy (depending only on its sign):

$$e^{2i\delta_j} = \frac{j}{\gamma - i\alpha_\epsilon}\frac{\Gamma(1+\gamma-i\alpha_\epsilon)}{\Gamma(1+\gamma+i\alpha_\epsilon)}e^{i\pi(j-\gamma)}; \quad \delta_j = \delta_{-j}. \tag{4.51}$$

Note that the general property (2.34) for massless fermions holds.

D. Scattering cross section

We start from the nonrelativistic limit, where one can directly sum the series (2.22) with S_m from Eq. (4.38) to obtain the nonrelativistic scattering amplitude in the closed form,[41,42]

$$f(\theta) = \frac{-i}{\sqrt{2p\sin^2(\theta/2)}}\frac{\Gamma\left(\frac{1}{2}-i\alpha_{\rm nr}\right)}{\Gamma(i\alpha_{\rm nr})}e^{i\alpha_{\rm nr}\ln\sin^2(\theta/2)}. \tag{4.52}$$

For completeness, the details are given in Appendix A. Using the property $\Gamma(z)\Gamma(1-z)=\pi/\sin(\pi z)$, the 2D Rutherford cross section follows,[41,42]

$$\frac{d\Lambda_{\rm nr}}{d\theta} = \frac{\alpha_{\rm nr}\tanh\pi\alpha_{\rm nr}}{2p\sin^2\dfrac{\theta}{2}}. \tag{4.53}$$

Here, θ is the scattering angle, and the momentum transfer $q=2p\sin\frac{\theta}{2}$. The cross section (4.53) is written in terms of the nonrelativistic fine structure constant (4.36).

In the opposite, massless limit, the phases (4.51) become independent on the absolute magnitude $|\epsilon|$ of energy. Thus, the differential scattering cross section scales with the particle wavelength,

$$\left.\frac{d\Lambda}{d\theta}\right|_{|\epsilon|\gg M} = \frac{\tau(\theta)}{|\epsilon|}, \tag{4.54}$$

where $\tau(\theta)$ is an $|\epsilon|$-independent function of the scattering angle. As the symmetry (2.34) is fulfilled, the backscattering is absent: $f(\pi)=0$ and $\tau(\pi)=0$, cf. Eq. (2.35).

For the general case, the differential cross section is obtained by summing the series (2.30) with S_j from Eq. (4.31). This problem is notoriously cumbersome, as it has long been known from the three dimensions.[33] Unfortunately, for the full relativistic problem ($Mv^2\neq\infty$), neither the differential nor the transport cross section can be obtained in the closed form. Moreover, the series (2.30) for the total cross section with the phase shifts (4.31) does not converge. To obtain the converging expression for the scattering amplitude, one needs to perform an appropriate resummation of this series.[33,46] In Appendix B, we show how to represent the Rutherford scattering amplitude via the convergent double integral, where the energy and angular dependences are separated. In the following section, we numerically sum the series (2.33) for the transport cross section.

V. EXACT COULOMB TRANSPORT CROSS SECTION IN GRAPHENE

For a half-filled π-electron band, the RPA screening (4.5) is scale invariant, preserving the *functional form* of the potential. This is why the exact solution for the Coulomb potential [Eq. (4.1)] can be practically important, as it survives the interaction effects at least on the linear screening level.

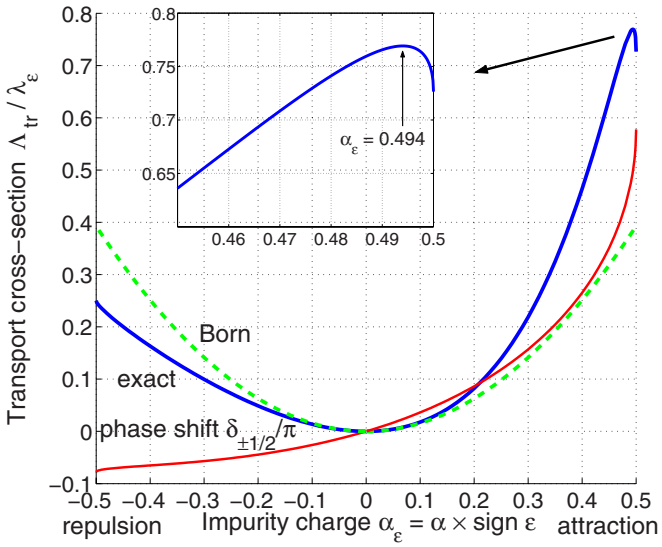

FIG. 2. (Color online) Transport cross section as a function of the impurity charge α (solid line). Dashed line is the Born approximation; thin red line is the lowest scattering phase shift $\delta_{\pm1/2}/\pi$ for $|j|=1/2$. Note that $\delta_{\pm1/2}=\pi/2$ (the unitary limit) for $\alpha\,\text{sgn}\,\epsilon=\alpha_\epsilon^*\approx0.494$; the transport cross section *decreases* for $\alpha_\epsilon^*<\alpha_\epsilon<1/2$, as shown in the inset. Attraction here means mutual attraction between the charged carrier and the impurity, i.e., sgn α=sgn ϵ, while repulsion stands for sgn α=−sgn ϵ.

The knowledge of the scattering phases (4.51) allows us to obtain the exact transport cross section (2.33) for scattering off the Coulomb impurity located in the immediate vicinity of the graphene sheet. Since the phase shifts are energy independent for $M=0$, the transport cross section is proportional to the energy-dependent carrier wavelength λ_ϵ,

$$\Lambda_{\rm tr} = C(\alpha_\epsilon)\lambda_\epsilon, \quad \lambda_\epsilon = 2\pi\hbar v/|\epsilon|. \tag{5.1}$$

The dimensionless function $C(\alpha_\epsilon)$ ($\alpha_\epsilon=\alpha\,\text{sign}\,\epsilon$), which is the transport cross section in the units of the carrier wavelength, is plotted in Fig. 2.

The transport cross section (5.1) has a few distinct features: (i) It is *not symmetric* with respect to the sign of the potential as seen by the carrier. A positively charged impurity ($\alpha>0$) scatters conduction electrons ($\epsilon>0$) more effectively than it scatters holes ($\epsilon<0$). The scattering asymmetry with respect to the sign of the potential arises naturally (e.g., in the next-to-leading Born approximation for low-energy particles, problem 6 in Sec. 132 of Ref. 39). Physically, one may expect the particle to spend more time around an attractive potential center and thereby be more significantly deflected (although for an ultrarelativistic particle this intuition may fail). However, for the practically important 2D and 3D Coulomb scattering in a parabolic band, the corresponding exact solutions are somewhat exceptional in a sense that they lack such an asymmetry. Remarkably, for the relativistic carrier dispersion, characteristic of graphene, this generally expected asymmetry is recovered. (ii) The cross section is ap-

parently *nonmonotonic* for the attractive Coulomb scatterers. (iii) The *unitary limit*, $\delta_{|j|=1/2}=\pi/2$ for the $j=\pm\frac{1}{2}$ partial wave, is reached for the mutual attraction when

$$\alpha_{\epsilon}^{*} \equiv \alpha \operatorname{sgn} \epsilon \approx 0.494, \tag{5.2}$$

just below criticality.

We were not able to link the above unitarity to any resonance or other special behavior at the point (5.2), which may as well be accidental. (One may argue that after subtracting the logarithmically divergent Coulomb phase, the phase shifts alone have lost their meaning, whereas the differences between them correspond to observable quantities.) Indeed, the partial Coulomb scattering phases δ_j even in the nonrelativistic Rutherford problem[39] generally pass the value $\pi/2$ at nonspecial values of parameters. At that point, the particular angular momentum channel reaches unitarity (maximum possible scattering). However, in previously studied cases, this unitarity in one channel did not cause a local maximum for the sum (2.24) over all channels. The opposite situation apparently happens in the 2D Dirac case: the relatively strong dependence of the scattering cross section on the lowest-j phase shift causes the local maximum shown in Fig. 2 inset.

The conductivity of graphene monolayer in the presence of charged impurities with the transport cross section (5.1) is obtained in Ref. 48. The attraction-repulsion asymmetry of the cross section can in principle allow one to determine the numbers of positively and negatively charged impurites independently.

Born approximation

We would now like to compare the exact result obtained above with the previously used Born approximation.[15–17] The Born scattering amplitude (2.44) is straightforwardly found using $U_{\mathbf{q}}=-2\pi\hbar v\alpha/q$:

$$f^{\mathrm{Born}}(\theta) = \alpha\sqrt{\frac{\pi}{8p}}\frac{1+e^{-i\theta}}{\sin(\theta/2)}. \tag{5.3}$$

Thus, the differential cross section

$$\frac{d\Lambda^{\mathrm{Born}}}{d\theta} = \frac{\pi\alpha^2}{2p}\cot^2\frac{\theta}{2}, \tag{5.4}$$

and the transport cross section

$$\Lambda_{\mathrm{tr}}^{\mathrm{Born}} = \frac{\pi^2\alpha^2}{p} \equiv C^{\mathrm{Born}}(\alpha)\lambda_{\epsilon}, \quad C^{\mathrm{Born}} = \frac{1}{2}\pi\alpha^2. \tag{5.5}$$

Note that the differential cross section is singular for $\theta=0$ as is expected from the long-range character of the Coulomb field.

The above cross sections can also be obtained from the Golden rule. For completeness, we present such a calculation for the momentum-relaxation time in the presence of n_i Coulomb impurities per unit area:

$$\frac{\hbar}{\tau_{\mathrm{tr}}^{\mathrm{Born}}(\epsilon)} = 2\pi n_i\int\frac{d^2\mathbf{p}'}{(2\pi\hbar)^2}|\mathcal{M}_{\mathbf{pp}'}|^2\delta(\epsilon_{\mathbf{p}}-\epsilon_{\mathbf{p}'})(1-\cos\theta)$$
$$= n_i\pi^2(Ze_*^2)^2/\epsilon \to n_i\pi^2(\hbar v\alpha)^2/\epsilon, \tag{5.6}$$

where the intraband matrix element of the interaction taken between the spinor plane wave states (1.9) is

$$\mathcal{M}_{\mathbf{pp}'} = \int d\mathbf{r}\,\psi_{\epsilon;\mathbf{p}'}^{\dagger}U(r)\psi_{\epsilon;\mathbf{p}} = \frac{1}{2}(1+e^{i\theta})U_{\mathbf{q}}. \tag{5.7}$$

Here, the Fourier transform of the effective potential (4.1) is $U_{\mathbf{q}}=-2\pi Ze_*^2/q$, and in Eq. (5.6), we accounted for RPA screening via the procedure (4.5). The transport cross section (5.5) follows from $n_i v\tau_{\mathrm{tr}}\Lambda_{\mathrm{tr}}=1$. We remark in passing on the following curious observation specific for the Born approximation: The ultrarelativistic Coulomb transport rate (5.6) written in terms of the quasiparticle energy ϵ formally coincides with the corresponding nonrelativistic value in two dimensions, where $\epsilon=p^2/2m^*$.

We also note that, as it is generally expected for the potential scattering,[39] the Born approximation (5.5) overestimates the exact result for the repulsion and underestimates it for the attraction. Figure 2 shows that, numerically, Born approximation works well for $\alpha\lesssim 0.1$, while for the experimentally relevant values $\alpha\simeq 0.5$, it fails by about a factor of 2. On a qualitative level, since the Born scattering assumes small phase shifts, it fails to recognize the strong attraction-repulsion asymmetry, the unitary scattering occurring at the value (5.2), and the associated nonmonotonic dependence of the cross section for the mutually attracting carrier and impurity.

SUMMARY

In this work we have outlined in detail the elastic scattering theory for the (2+1)-dimensional massive Dirac fermions in an axially symmetric potential. The formalism is relevant for the transport in pristine graphene monolayers (massless limit) and for graphene layers with the broken symmetry between the sublattices (resulting in the finite Dirac mass gap), in the presence of a smooth potential disorder. We showed that the Dirac theory becomes sensitive to the lattice scale for the potentials that are more singular than $1/r$ as $r\to 0$. We also considered scattering off a localized potential whose size is smaller than the Dirac fermion wavelength (but larger than the graphene lattice scale). For the Coulomb scattering, $U=-\hbar v\alpha/r$, the exact solution is found below the threshold $|\alpha|<1/2$; from the scattering phase shifts, we obtain the exact transport cross section. The transport cross section for the massless case (pristine graphene) is shown to exhibit a pronounced asymmetry with respect to attraction versus repulsion between the charge carrier and the Coulomb impurity.

Note added: Recently, we learned about the preprint[49] where, for the Coulomb potential, the opposite, supercritical situation $|\alpha|>1/2$ is discussed for the massless limit. The perturbative renormalization group treatment of Ref. 49, based on the single-particle Friedel sum rule, applies in the weakly interacting limit $e_*^2/\hbar v\ll 1$. The strong-coupling

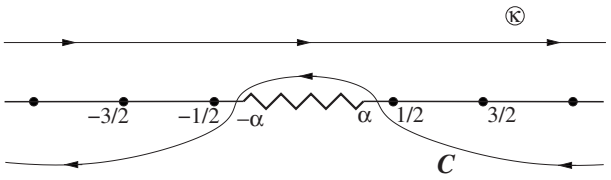

FIG. 3. The contour $\mathcal{C}$ of integration in the complex κ plane for summing over $\kappa=\pm 1/2, \pm 3/2, \ldots$.

limit of the problem, valid for $e_*^2/\hbar v \sim 1$ and large impurity charge $Z \gg 1$, was subsequently considered in Ref. 50, yielding a qualitative change in the screened potential profile. Also, recently, angular resolved photoemission spectroscopy measurement[51] became available, according to which the Dirac gap $\Delta \sim 0.1$ eV opens up for graphene on SiC substrate. In the presence of Coulomb impurities, this would lead to the subgap states (4.19) with the wave function spread over ~ 10 nm [cf. Eq. (4.23)]. Localized states on this length scale can be detected using scanning techniques.

ACKNOWLEDGMENTS

It is a pleasure to thank L. Glazman, M. Voloshin, B. Shklovskii, and A. Shytov for helpful discussions. This work was supported by NSF MRSEC Grant No. DMR 02-13706 (at Princeton) and NSF Grants No. DMR 02-37296 and DMR 04-39026 (at FTPI).

APPENDIX A: NONRELATIVISTIC COULOMB SCATTERING AMPLITUDE

Here, we show how to sum the series (2.22) with S_m from Eq. (4.38). For that, we first use the integral representation

$$\frac{\Gamma\left(m+\frac{1}{2}-i\alpha_{\rm nr}\right)}{\Gamma\left(m+\frac{1}{2}+i\alpha_{\rm nr}\right)} = \frac{\mathrm{B}\left(m+\frac{1}{2}-i\alpha_{\rm nr}, 2i\alpha_{\rm nr}\right)}{\Gamma(2i\alpha_{\rm nr})} = \frac{1}{\Gamma(2i\alpha_{\rm nr})}\int_0^1 dt\, t^{m-1/2-i\alpha_{\rm nr}}(1-t)^{2i\alpha_{\rm nr}-1}. \tag{A1}$$

Noting that $S_{-m}^{\rm nr}=S_m^{\rm nr}$, we then sum the two similar looking geometric series. Defining $z=e^{i\theta}$, we find

$$\sum_{m=0}^{\infty} S_m z^m + \sum_{m=1}^{\infty} S_m z^{-m} = \frac{\Gamma\left(\frac{1}{2}-i\alpha_{\rm nr}\right)}{\Gamma\left(\frac{1}{2}+i\alpha_{\rm nr}\right)}\tilde{\mathcal{F}}\left(1, \tfrac{1}{2}-i\alpha_{\rm nr}, \tfrac{1}{2}+i\alpha_{\rm nr}; z\right) + \frac{\Gamma\left(\frac{3}{2}-i\alpha_{\rm nr}\right)}{\Gamma\left(\frac{3}{2}+i\alpha_{\rm nr}\right)}\frac{1}{z}\tilde{\mathcal{F}}\left(1, \tfrac{3}{2}-i\alpha_{\rm nr}, \tfrac{3}{2}+i\alpha_{\rm nr}; z^{-1}\right). \tag{A2}$$

Here, we used the integral representation [Ref. 47, Eq. (9.111)]

$$\tilde{\mathcal{F}}(a,b,c;z) = \frac{1}{\mathrm{B}(b,c-b)}\int_0^1 dt\, t^{b-1}(1-t)^{c-b-1}(1-zt)^{-a} \tag{A3}$$

for the hypergeometric function

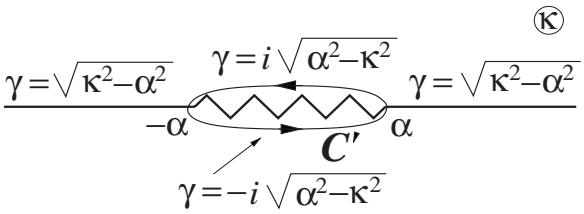

FIG. 4. The final contour $\mathcal{C}'$ of integration in the complex κ plane.

$$\tilde{\mathcal{F}}(a,b,c;z) = 1 + \frac{ab}{c}\frac{z}{1!} + \frac{a(a+1)b(b+1)}{c(c+1)}\frac{z^2}{2!} + \cdots. \tag{A4}$$

Now, we use the analytic continuation of the hypergeometric series for $|z|>1$, Eq. (9.132.2) of Ref. 47 [Eq. (e.6) of Ref. 39],

$$\tilde{\mathcal{F}}(a,b,c;z) = \frac{\Gamma(c)\Gamma(b-a)}{\Gamma(b)\Gamma(c-a)}(-z)^{-a} \times \tilde{\mathcal{F}}(a,a+1-c,a+1-b;z^{-1}) + \frac{\Gamma(c)\Gamma(a-b)}{\Gamma(a)\Gamma(c-b)}(-z)^{-b}\tilde{\mathcal{F}}(b,b+1-c,b+1-a;z^{-1}), \tag{A5}$$

to transform the second term of Eq. (A2) to become the function of z rather than z^{-1}. Application of the first term of formula (A5) cancels the first term of sum (A2), while the second term of Eq. (A5) yields

$$\sum_{m=-\infty}^{\infty} S_m z^m = -\frac{\Gamma\left(-\frac{1}{2}+i\alpha_{\rm nr}\right)\Gamma\left(\frac{3}{2}-i\alpha_{\rm nr}\right)}{\Gamma(2i\alpha_{\rm nr})}(-z^{-1})^{-1/2+i\alpha_{\rm nr}} \times \tilde{\mathcal{F}}\left(\tfrac{3}{2}-i\alpha_{\rm nr}, 1-2i\alpha_{\rm nr}, \tfrac{3}{2}-i\alpha_{\rm nr}; z\right). \tag{A6}$$

Finally, using Eq. (9.131) of Ref. 47 [Eq. (e.4) of Ref. 39],

$$\tilde{\mathcal{F}}(a,b,c;z) = (1-z)^{c-a-b}\tilde{\mathcal{F}}(c-a,c-b,c;z), \tag{A7}$$

as well as the doubling formula [Ref. 47, Eq. (8.335.1)]

$$\Gamma(2x) = \frac{2^{2x-1}}{\sqrt{\pi}}\Gamma(x)\Gamma\left(x+\frac{1}{2}\right), \tag{A8}$$

and $-(1-z)^2/z = 4\sin^2(\theta/2)$, one obtains the scattering amplitude (4.52).

APPENDIX B: RELATIVISTIC COULOMB SCATTERING AMPLITUDE

Consider the following transformations of the series for the scattering amplitude (2.30), $z \equiv e^{i\theta}$:

$$\sum_{m=-\infty}^{\infty} S_m z^m = z^{-1/2} \sum_{j=\pm 1/2,\pm 3/2,\ldots,} z^j (j + i\tilde{M}) \frac{\Gamma(\gamma - i\alpha_\epsilon)}{\Gamma(1+\gamma+i\alpha_\epsilon)} e^{i\pi(j-\gamma)} \tag{B1a}$$

$$= \frac{z^{-1/2}}{\Gamma(1+2i\alpha_\epsilon)} \int_0^1 dt\, t^{-i\alpha_\epsilon} (1-t)^{2i\alpha_\epsilon} \times \int_{\mathcal{C}} \frac{d\kappa}{2\pi i} \pi \tan(\pi\kappa)(\kappa + i\tilde{M}) z^\kappa t^{\gamma-1} e^{i\pi(\kappa-\gamma)} \tag{B1b}$$

$$= -\frac{z^{-1/2}}{\Gamma(1+2i\alpha_\epsilon)} \int_0^1 dt \frac{d}{dt} \{t^{-i\alpha_\epsilon}(1-t)^{2i\alpha_\epsilon}\} \times \int_{\mathcal{C}'} \frac{d\kappa}{2\pi i} \frac{\pi \tan(\pi\kappa)}{\gamma(\kappa)} (\kappa + i\tilde{M}) z^\kappa t^\gamma e^{i\pi(\kappa-\gamma)}. \tag{B1c}$$

Here, $\tilde{M} \equiv \alpha M/p$, and in the first line, we canceled the denominator $\gamma - i\alpha_\epsilon$ by utilizing the property $\Gamma(x+1) = x\Gamma(x)$.

In the next line, Eq. (B1b), we utilize the integral representation for the Euler's beta function,

$$\mathrm{B}(p,q) = \frac{\Gamma(p)\Gamma(q)}{\Gamma(p+q)} = \int_0^1 dt\, t^{p-1}(1-t)^{q-1}. \tag{B2}$$

The summation is reduced to the contour integration by virtue of the fact that $\pi \tan \pi\kappa$ has residues at the points $\kappa = \pm 1/2, \pm 3/2, \ldots$, with a value -1. The κ integration is along the contour $\mathcal{C}$ shown in Fig. 3.

Finally, in Eq. (B1c), we have performed the integration by parts in the t variable, $t^{\gamma-1} = d(t^\gamma)/\gamma$. In this way all the remaining singular behavior in the κ plane (besides the residues at $\kappa = \pm 1/2, \pm 3/2, \ldots$) is reduced to that of $\gamma(\kappa)$ in the denominator. The phase of the square root in $\gamma(\kappa) = \sqrt{\kappa^2 - \alpha^2}$ is defined in a standard way, Fig. 4. The exponential function $e^{i\pi(\kappa-\gamma)}$ does not diverge for large imaginary κ, which allows us to deform the integration contour $\mathcal{C}$ in Eq. (B1) to $\mathcal{C}'$ around the cut between $\kappa = \pm\alpha$ shown in Fig. 4. Clearly, this procedure is valid only if condition (4.3) is satisfied.

[1] P. R. Wallace, Phys. Rev. **71**, 622 (1947).
[2] J. W. McClure, Phys. Rev. **104**, 666 (1956).
[3] R. Saito, G. Dresselhaus, and M. S. Dresselhaus, *Physical Properties of Carbon Nanotubes* (Imperial College Press, London, 1998).
[4] G. W. Semenoff, Phys. Rev. Lett. **53**, 2449 (1984).
[5] F. D. M. Haldane, Phys. Rev. Lett. **61**, 2015 (1988).
[6] K. S. Novoselov, A. K. Geim, S. V. Morozov, D. Jiang, Y. Zhang, S. V. Dubonos, I. V. Grigorieva, and A. A. Firsov, Science **306**, 666 (2004); K. S. Novoselov, D. Jiang, F. Schedin, T. J. Booth, V. V. Khotkevich, S. V. Morozov, and A. K. Geim, Proc. Natl. Acad. Sci. U.S.A. **102**, 10451 (2005).
[7] K. S. Novoselov, A. K. Geim, S. V. Morozov, D. Jiang, M. I. Katsnelson, I. V. Grigorieva, S. V. Dubonos, and A. A. Firsov, Nature (London) **438**, 197 (2005); K. S. Novoselov, E. McCann, S. V. Morozov, V. I. Fal'ko, M. I. Katsnelson, U. Zeitler, D. Jiang, F. Schedin, and A. K. Geim, Nat. Phys. **2**, 177 (2006).
[8] C. Berger, Z. Song, T. Li, X. Li, A. Y. Ogbazghi, R. Feng, Z. Dai, A. N. Marchenkov, E. H. Conrad, P. N. First, and W. A. de Heer, J. Phys. Chem. B **108**, 19912 (2004).
[9] Y. Zhang, J. P. Small, M. E. S. Amori, and P. Kim, Phys. Rev. Lett. **94**, 176803 (2005); Y. Zhang, Y.-W. Tan, H. L. Stormer, and P. Kim, Nature (London) **438**, 201 (2005).
[10] A. K. Geim and K. S. Novoselov, Nat. Mater. **6**, 183 (2007).
[11] D. P. DiVincenzo and E. J. Mele, Phys. Rev. B **29**, 1685 (1984).
[12] N. H. Shon and T. Ando, J. Phys. Soc. Jpn. **67**, 2421 (1998).
[13] H. Suzuura and T. Ando, Phys. Rev. Lett. **89**, 266603 (2002).
[14] N. M. R. Peres, F. Guinea, and A. H. Castro Neto, Phys. Rev. B **73**, 125411 (2006).
[15] T. Ando, J. Phys. Soc. Jpn. **75**, 074716 (2006).
[16] K. Nomura and A. H. MacDonald, Phys. Rev. Lett. **96**, 256602 (2006).
[17] E. H. Hwang, S. Adam, and S. Das Sarma, Phys. Rev. Lett. **98**, 186806 (2007).
[18] P. M. Ostrovsky, I. V. Gornyi, and A. D. Mirlin, Phys. Rev. B **74**, 235443 (2006).
[19] M. I. Katsnelson, Phys. Rev. B **74**, 201401(R) (2006).
[20] D. V. Khveshchenko, Phys. Rev. Lett. **97**, 036802 (2006).
[21] E. McCann, K. Kechedzhi, V. I. Fal'ko, H. Suzuura, T. Ando, and B. L. Altshuler, Phys. Rev. Lett. **97**, 146805 (2006).
[22] A. F. Morpurgo and F. Guinea, Phys. Rev. Lett. **97**, 196804 (2006).
[23] V. V. Cheianov and V. I. Fal'ko, Phys. Rev. Lett. **97**, 226801 (2006).
[24] I. L. Aleiner and K. B. Efetov, Phys. Rev. Lett. **97**, 236801 (2006).
[25] A. Altland, Phys. Rev. Lett. **97**, 236802 (2006).
[26] M. I. Katsnelson and K. S. Novoselov, Solid State Commun. **143**, 3 (2007).
[27] M. Hentschel and F. Guinea, Phys. Rev. B **76**, 115407 (2007).
[28] G. Giovannetti, P. A. Khomyakov, G. Brocks, P. J. Kelly, and J. van den Brink, Phys. Rev. B **76**, 073103 (2007).
[29] E. McCann and V. I. Fal'ko, Phys. Rev. Lett. **96**, 086805 (2006); E. McCann, Phys. Rev. B **74**, 161403(R) (2006).
[30] J. Nilsson, A. H. Castro Neto, N. M. R. Peres, and F. Guinea, Phys. Rev. B **73**, 214418 (2006); F. Guinea, A. H. Castro Neto, and N. M. R. Peres, *ibid.* **73**, 245426 (2006); J. Nilsson and A. H. Castro Neto, Phys. Rev. Lett. **98**, 126801 (2007).
[31] T. Ohta, A. Bostwick, T. Seyller, K. Horn, and E. Rotenberg, Science **313**, 951 (2006).
[32] C. L. Kane and E. J. Mele, Phys. Rev. Lett. **95**, 226801 (2005).
[33] V. B. Berestetskii, E. M. Lifshits, and L. P. Pitaevskii, *Quantum Electrodynamics* (Elsevier, Oxford, 1971).
[34] V. R. Khalilov and C. L. Ho, Mod. Phys. Lett. A **13**, 615 (1998).
[35] I. Pomeranchuk and Ya. Smorodinsky, J. Phys. (USSR) **9**, 97 (1945).
[36] S. S. Gershtein and Ya. B. Zeldovich, Zh. Eksp. Teor. Fiz. **57**, 654 (1969) [Sov. Phys. JETP **30**, 358 (1970)].

[37] V. S. Popov, Yad. Fiz. **12**, 429 (1970) [Sov. J. Nucl. Phys. **12**, 235 (1971)].
[38] Ya. B. Zeldovich and V. S. Popov, Usp. Fiz. Nauk **105**, 403 (1971) [Sov. Phys. Usp. **14**, 673 (1972)].
[39] L. D. Landau and E. M. Lifshits, *Quantum Mechanics (Non-relativistic Theory)* (Elsevier, Oxford, 1977).
[40] J. Schwinger, Phys. Rev. **82**, 664 (1951).
[41] F. Stern and W. E. Howard, Phys. Rev. **163**, 816 (1967).
[42] G. Barton, Am. J. Phys. **51**, 420 (1983).
[43] T. Ando, T. Nakanishi, and R. Saito, J. Phys. Soc. Jpn. **67**, 2857 (1998).
[44] J. Gonzalez, F. Guinea, and M. A. H. Vozmediano, Phys. Rev. B **59**, R2474 (1999).
[45] B. Zaslow and M. E. Zandler, Am. J. Phys. **35**, 1118 (1967).
[46] R. L. Gluckstern and S.-R. Lin, J. Math. Phys. **5**, 1594 (1964).
[47] I. S. Gradshteyn and I. M. Ryzhik, *Table of Integrals, Series, and Products*, 6th ed. (Academic, New York, 2000).
[48] D. S. Novikov, Appl. Phys. Lett. **91**, 102102 (2007).
[49] A. V. Shytov, M. I. Katsnelson, and L. S. Levitov, arXiv:0705.4663 (unpublished).
[50] M. M. Fogler, D. S. Novikov, and B. I. Shklovskii, Phys. Rev. B **76**, 233402 (2007).
[51] S. Y. Zhou, G.-H. Gweon, A. V. Fedorov, P. N. First, W. A. de Heer, D.-H. Lee, F. Guinea, A. H. Castro Neto, and A. Lanzara, Nat. Mater. **6**, 770 (2007).